SOIL, 9, 189–208, 2023
https://doi.org/10.5194/soil-9-189-2023

SOIL Open Access EGU

Masked diversity and contrasting soil processes in tropical seagrass meadows: the control of environmental settings

Gabriel Nuto Nóbrega[1], Xosé L. Otero[2], Danilo Jefferson Romero[3], Hermano Melo Queiroz[3], Daniel Gorman[4], Margareth da Silva Copertino[5], Marisa de Cássia Piccolo[6], and Tiago Osório Ferreira[3]

[1]Department of Soil Sciences, Federal University of Ceará, Av. Mister Hull, 2977, Campus do Pici, 60356-001, Fortaleza, Ceará, Brazil
[2]Cretus, Departamento de Edafoloxía e Química Agrícola, Facultade de Bioloxía, Universidade de Santiago de Compostela, Rúa Lope G Marzoa, s/n, Campus sur. 15782, Santiago de Compostela, Spain
[3]Department of Soil Science, College of Agriculture Luiz de Queiroz, University of São Paulo, ESALQ/USP, Av. Pádua Dias 11, 13.418-260, Piracicaba, São Paulo, Brazil
[4]Commonwealth Scientific and Industrial Research Organization (CSIRO), Environment, Crawley, WA, Australia
[5]Institute of Oceanography, Federal University of Rio Grande (FURG), Av. Itália Km 08, Carreiros, Rio Grande – RS, CEP: 96.201-900, Brazil
[6]Laboratory of Nutrient Cycling, Center of Nuclear Energy in Agriculture, University of São Paulo, Av. Centenário 303, 13.400.970, Piracicaba, São Paulo, Brazil

Correspondence: Tiago Osório Ferreira (toferreira@usp.br)

Received: 9 June 2022 – Discussion started: 27 July 2022
Revised: 1 December 2022 – Accepted: 3 February 2023 – Published: 16 March 2023

Abstract. Seagrass meadows are among the most valuable ecosystems on Earth. However, in tropical countries, there is a substantial knowledge gap in "seagrass science". To address this gap, seagrass soils from three Brazilian coastal regions were investigated (the northeastern, southeastern, and southern coasts). Soil profiles from different geological and bioclimatic settings were sampled, described, and analyzed. Thus, detailed macromorphological descriptions, soil classification, physicochemical analysis (soil particle size, soil pH, $pH_{oxidation}$, E_h, total organic carbon: TOC), Fe partitioning, and X-ray diffractometry were performed. Additionally, water samples were analyzed for pH, salinity, and ion concentrations. Different environmental settings in the coastal compartments produced contrasting geochemical conditions, which caused different intensities of pedogenetic processes. On the northeastern coast, the denser plant coverage favored higher TOC contents (2.5 ± 0.1 %) and an anaerobic environment ($E_h = +134 \pm 142$ mV) prone to an intense sulfidization (i.e., pyrite formation: Py-Fe). Py-Fe contents in northeastern soils were 6- and 2-fold higher than in southeastern and southern coastal soils, respectively. Conversely, lower TOC contents (0.35 ± 0.15 %) and a suboxic environment ($E_h + 203 \pm 55$ mV) in the southeastern soils, along with the Fe-rich geological surroundings, decreased the intensity of gleization. The contrasting intensities in the soil processes, related to the (seemingly subtle) differences in the geochemistry of each environment, ultimately caused relevant pedodiversity among the studied sites. Our findings contribute to a better understanding of the general functioning of tropical seagrass meadows but also have significant environmental implications for studies focused on carbon sequestration in these ecosystems.

Published by Copernicus Publications on behalf of the European Geosciences Union.

1 Introduction

Seagrass meadows are ecosystems adapted to a wide range of environmental conditions, such as salinity, soil grain size composition, temperature, light, and water column depth (Copertino et al., 2016). Despite the low taxonomic diversity of plant species (approximately 14 genera and 60 species), the global distribution can range from 300 000 to 600 000 km^2, corresponding to 0.2 %–0.5 % of the ocean area (Fourqurean et al., 2012; da Silva Copertino, 2011). Seagrasses are distributed throughout the shallow coastal waters in temperate and tropical regions (Short et al., 2007) and found in more than 120 countries, with the most extensive areas in the United States, Australia, the Philippines, and India (Green and Short, 2003).

These ecosystems are recognized as highly productive (Duarte et al., 2005, 2010) and a source of nutrients (e.g., C, N, and P) to the adjacent areas and deep ocean (Short et al., 2011). Thus, these meadows are among the most important ecosystems on the planet, supporting several species at all trophic levels and providing numerous ecological services (Costanza et al., 2014; Orth et al., 2006). However, despite many of these ecosystem services being directly supported by their soils (e.g., carbon sequestration, nutrient provision, filtering of pollutants, and hosting biodiversity; Walker and McComb, 1992; Baden et al., 2012; Marbà et al., 2015; Zarnoch et al., 2017; Thorhaug et al., 2017), the comprehension of subaqueous soils as natural bodies is still scarce (Ferronato et al., 2016), regardless of the seminal pedological studies on temperate seagrasses conducted in the early 1990s (Demas, 1993; Demas et al., 1996).

In many tropical countries, there is a substantial knowledge gap in "seagrass science" (Ooi et al., 2011). In Brazil, marked by an extensive (approximately 9200 km) and diverse coastline (Copertino et al., 2016), very few pedological studies have been conducted on seagrass meadows (Nóbrega, 2018). Brazil's latitudinal gradient provides a variety of climates, geological settings, and geomorphological environments and, thus, a unique framework for assessing soil diversity in tropical seagrass meadows. Although most studies on subaqueous soils worldwide have investigated soil–landscape relationships, hydrodynamics, and hydromorphism (Wessel et al., 2021; Vittori Antisari et al., 2016; Osher and Flannagan, 2007; Erich and Drohan, 2012; Bradley and Stolt, 2006, 2003), few have focused on how and to what extent contrasting soil-forming factors drive the variability of seagrass soils and their potential environmental implications.

The present work aimed to study the pedogenesis of seagrass soils under contrasting environmental conditions of three coastal regions of Brazil (the Northeastern Semiarid Coast, Southern Granitic Coast, and Southern Quaternary Coast). By studying seagrass soils under contrasting hydrological, geological, and bioclimatic settings, we sought to provide a better understanding of the diversity, formation, and functions of these subaqueous soils in the provision of key ecosystem services.

2 Material and methods

2.1 Study sites

Seagrass meadows located in three contrasting geomorphoclimatic regions along the Brazilian coast were studied: the Northeastern Semiarid Coast (northeastern coast), where samples were collected in the state of Ceará in the estuary of the Timonha River (Fig. 1), the Southern Granitic Coast (southeastern coast), where samples were collected in the state of São Paulo in the city of São Sebastião (Fig. 2), and the Southern Quaternary Coast (southern coast), where samples were collected in the state of Rio Grande do Sul, inside the world's largest choked lagoon (i.e., Patos Lagoon estuary; Fig. 3). The northeastern and southeastern coastal compartments are predominantly vegetated by *Halodule* spp. (tropical marine species), whereas the euryhaline *Ruppia maritima* inhabits the southern coast (Fig. S1 in the Supplement). On the northeastern coast, the seagrass meadows were characterized by dense vegetation under low anthropogenic impacts and at water depths ranging from 1.7 to 2.9 m (water column during sampling approximately 2 m, collected during low tide). In the southeast, the sampled seagrass meadows were marked by lower plant densities and grew at a mean water depth of 1.3 m (water column during sampling approximately 1.6 m, collected during low tide). The southern coast seagrass meadows were colonized by *Ruppia maritima* and are marked by low-density vegetation and a mean water depth of 1.3 m (water column during sampling approximately 1.5 m, collected during low tide).

The northeastern coast, which stretches from the states of Piauí to Pernambuco, is characterized by a semiarid climate (the Aw and Bhs climate types according to the Köppen–Geiger climate classification; Fig. 1; Peel et al., 2007), with an annual rainfall of 700–1000 mm and high potential evapotranspiration rates of 1500–1600 mm (Alvares et al., 2013). Seagrasses on the northeastern coast are subject to a mesotidal regime and low riverine discharges ($< 1000^3\ s^{-1}$; Schaeffer-Novelli et al., 1990). The geological setting is characterized by the Barreiras Formation, a Miocene–Pliocene extensive sedimentary deposit (Dominguez, 2006) predominantly composed of fine to coarse sands, gray-reddish, purple, and yellowish clays, and poorly sorted gray-whitish, yellow, and coarse to conglomeratic sandstones with a kaolinite matrix (Vilas Bôas et al., 2001). Soils from the Barreiras Formation are mostly Lixisols and Acrisols (Bezerra et al., 2015).

The southeastern granitic coast covers an area from the states of Rio de Janeiro (Guanabara Bay) to Santa Catarina (Praia dos Sonhos). In this coastal region, seagrasses are mostly subject to a microtidal regime and a humid tropical climate (CWa according to the Köppen–Geiger climate clas-

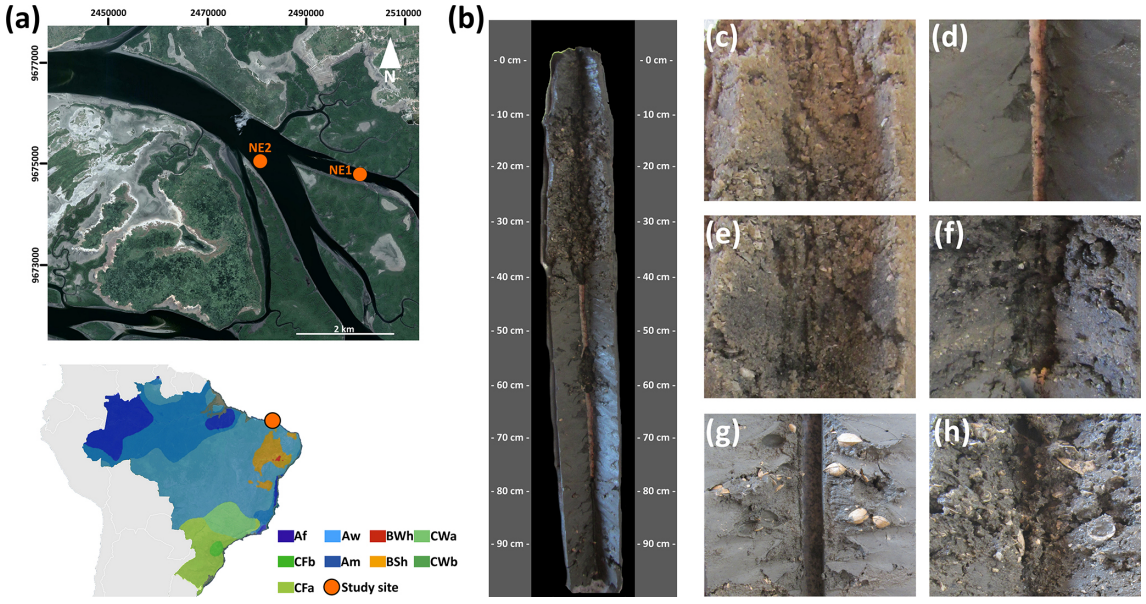

Figure 1. **(a)** Sampling site location on the northeastern Brazilian coast and the Köppen–Geiger climatic classification of the studied sites (source: Peel et al., 2007). **(b)** The representative soil profile of the northeastern coast (NE1; soil horizons: Arz 0–10 cm, CArz 10–26 cm, Crz1 26–37 cm, Crz2 37–56 cm, 2Crz 56–84 cm, 3Crnz 84–114 cm) classified as a Eutric Fluvic Reductigleyic Subaquatic Gleysol (Loamic, Hypersalic, Sodic, Hypersulfidic). Detailed images in panels **(c)** and **(d)** of the contrast between the massive and single-grained grades in horizons 3Crnz and Crz2, respectively. **(e)** Coarse soil texture (fine sandy loam) in the Crz2 horizon. **(f)** Lowermost 3Crnz horizon with black-colored spots in the soil matrix due to metal sulfides. Panels **(g)** and **(h)** show intact and fragmented seashells in the Crz1 soil horizon.

sification; Fig. 2; Peel et al., 2007), with a mean annual rainfall of > 2000 mm for 150–170 d (i.e., rainy season), resulting in a considerable hydric surplus (Minuzzi et al., 2007; Banco de dados climáticos do Brasil, 2019). The coastal plain is narrow and surrounded by a Precambrian mountain range (i.e., Serra do Mar outcrops) composed of crystalline massifs of granite–gneiss rocks (Dominguez, 2006; Schaeffer-Novelli et al., 1990; Reverte and Garcia, 2016). The surrounding soils are mainly Cambisols, Acrisols, Podzols, and Arenosols (Furlan et al., 2011).

The southern coast extends 600 km south of the granitic coast to the border with Uruguay. This coast has a temperate climate (CFa according to the Köppen–Geiger climate classification; Fig. 3; Peel et al., 2007) with low mean annual temperatures (approximately 18 °C during winter and 23–28 °C during summer) and a hydric surplus of approximately 400 mm (Schaeffer-Novelli et al., 1990; Bernardino et al., 2015). The seagrass meadows in this coastal region were subject to a microtidal regime. The geology is characterized by sandy deposits related to Quaternary transgressive events (Toldo Jr. et al., 2000). The dominant soils in the southern river basins are mainly Fluvisols and Planosols (Lemos et al., 1973).

2.2 Soil and water sampling

Preliminary soil sampling was performed at all the sites to better assess the spatial variation in the studied compartments. Based on the local soil variation, each compartment's most representative and permanently submerged soil profiles were selected. Data corresponding to six representative profiles (two at each study site) are presented for the present study. Soil profiles were sampled using transparent polycarbonate tubes (1.5 m length, 90 mm diameter) attached to an auger for submerged soils (Supplement; Nóbrega et al., 2018). After sampling, the soil cores were carefully removed from the tubes, and the soil profiles were morphologically described (Fig. S2) according to the FAO/WRB guidelines (Jahn et al., 2006) within 1 to 2 h to minimize atmospheric interference and sample oxidation. Water samples were collected at each study site (in triplicate) using pre-rinsed polyethene bottles, which were cooled until analysis.

After the morphological description, the soil profiles were sectioned according to the identified soil horizons. The pH_{field}, redox potential (E_h), and electrical conductivity (EC) were measured in situ in each soil horizon using portable electrodes immediately after removing the soil cores from the tubes. The pH_{field} and EC were determined using calibrated glass electrodes (Hannah HI 9025), and E_h was obtained using a platinum electrode (Hannah HI 9025) by directly inserting the probes into the soil. The final E_h readings were corrected by adding the potential of the calomel

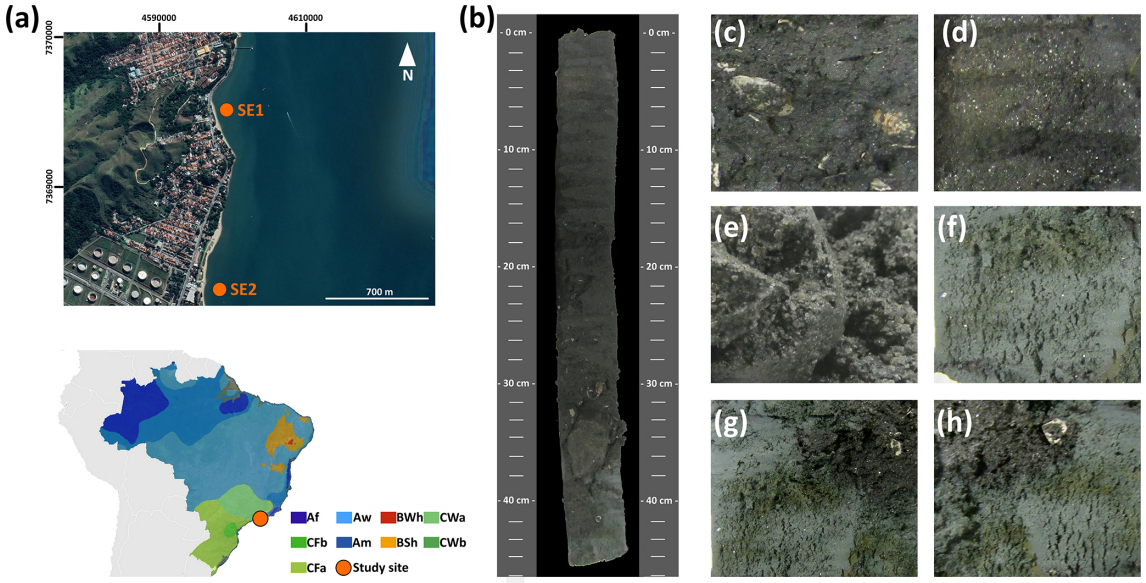

Figure 2. **(a)** Sampling site location on the southeastern Brazilian coast and the Köppen–Geiger climatic classification of the studied sites (source: Peel et al., 2007). **(b)** The representative soil profile of the southeastern coast (SE2, soil horizons: Arz 0–5 cm, ACrz 5–12 cm, Crz 12–26 cm, Crnz 26–33 cm, 2Crzn1 33–42 cm, 2Crz2 42–47 cm, 2Crz3 47–50+ cm) classified as a Eutric Fluvic Reductigleyic Subaquatic Gleysol (Loamic, Hypersalic, Sodic, Hyposulfidic). Detailed images of **(c)** fragmented seashells in the 2Crz1 soil horizon, **(d)** mica-like grain morphology in the surface horizons of the soil profile (feature produced by sediment inputs from the surrounding crystalline rocks), **(e)** coarse soil texture (loamy coarse sand) in the ACrz horizon, **(f)** finer soil texture (coarse sandy loam) in the 2Crz3 horizon, and **(g)** and **(h)** very dark greenish gray colors (10BG 3/1) in the Crnz soil horizon.

reference electrode (+244 mV) (Nóbrega et al., 2014; Otero et al., 2009). Then, samples were transferred in plastic bags and stored at approximately 4 °C in the laboratory.

In the laboratory, subsamples were frozen (named "fresh samples"), whereas the remaining subsamples were pretreated with ethanol (60 %) to remove soluble salts until the silver nitrate test (0.05 mol L^{-1} $AgNO_3$) indicated the absence of chlorides. After the removal of soluble salts, samples were dried (45 °C) and sieved (2 mm) for chemical (i.e., exchangeable cation) and physical (i.e., particle size distribution) analyses (Bower et al., 1952; Sumner and Miller, 2018).

2.3 Soil physical and chemical characterization

The particle size distribution was determined by the hydrometer method using a combination of chemical (0.015 mol L^{-1} $(NaPO_3)_6$ + 1.0 mol L^{-1} NaOH) and physical (16 h shaking) dispersion methods (Gee and Bauder, 1986). Samples were previously treated to remove organic matter (H_2O_2 30 %). Then, the sand was separated using a 0.053 mm sieve, and clay was separated from the silt by sedimentation based on Stokes' law.

Fresh soil subsamples were used to determine the total organic carbon (TOC) content, total potential acidity ($pH_{oxidation}$), calcium carbonate equivalent (CCE), and partitioning of Fe solid phases. The TOC content was determined by dry combustion using an elemental analyzer (LECO TruSpec CHNS). The fresh subsoil samples were pretreated to remove inorganic carbon with 1 mol L^{-1} HCl and then dried at 45 °C for TOC determination (Howard et al., 2014). The titrimetric method was applied to quantify the CCE (FAO, 2020). The $pH_{oxidation}$ was determined after the oxidation of fresh soil samples with hydrogen peroxide (30 %, pH 5.5; 1 soil: 5 solution) followed by pH measurement to test for the presence of sulfidic materials (IUSS Working Group WRB, 2015; Konsten et al., 1988).

The solid-phase Fe partitioning was obtained in 2 g of fresh soil samples using the method proposed by Lord III (1982), resulting in two distinct phases: Fe oxyhydroxides (Oxy-Fe), extracted with 20 mL of a 0.25 mol L^{-1} sodium citrate +0.11 mol L^{-1} sodium bicarbonate solution, with 3 g of sodium dithionite, at 75 °C for 30 min shaking. After the extraction of Oxy-Fe (i.e., before the extraction of pyritic Fe – Py-Fe), the residue was pretreated to remove Fe bound to phyllosilicates and organic matter using 10 mol L^{-1} HF (hydrofluoric acid) for 16 h under agitation and concentrated H_2SO_4 (2 h under agitation). Next, Py-Fe was extracted with 10 mL of concentrated HNO_3 shaking for 2 h at room temperature. Between each step, samples were centrifuged (6000 rpm at 4 °C) and washed with 20 mL ultrapure water. The Fe concentrations in the extracts were determined using an inductively coupled plasma optical emission spectrometer (Thermo Fisher Scientific, Waltham, MA, USA). For Fe determination, curve calibration solutions were prepared by

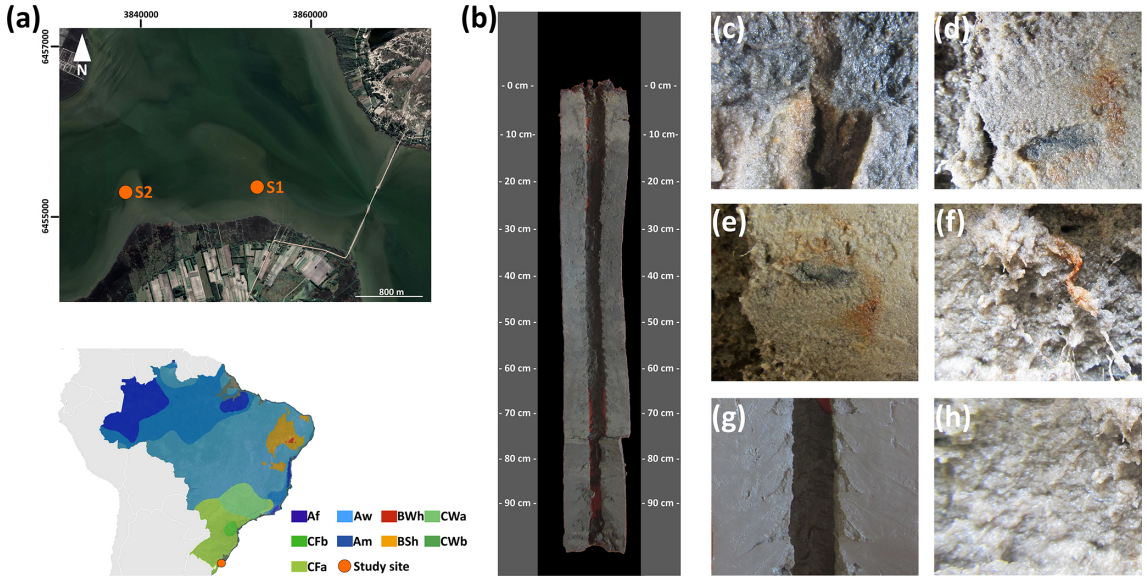

Figure 3. **(a)** Sampling site location on the southern Brazilian coast and the Köppen–Geiger climatic classification of the studied sites (source: Peel et al., 2007). **(b)** The representative soil profile of the southern coast (S1, soil horizons Ar 0–6 cm, ACrj 6–13 cm, CAr1 13–30 cm, CAr2 30–44 cm, Cr 44–70 cm, 2Crn1 70–93 cm, 2Crn1/2Crn2 93–106 cm, 2Crn2 106–111 cm) classified as a Eutric Fluvic Reductigleyic Subaquatic Gleysol (Loamic, Protosalic, Sodic, Hypersulfidic). Detailed images of **(c)** and **(d)** black-colored spots (10BG 3/1 very dark greenish gray) due to metal sulfides in the Crn2/2Crn, **(e)** and **(f)** brown mottles (7.5YR 4/4) associated with roots (oxyhydroxide precipitations), and **(g)** and **(h)** contrasting soil textures between horizons 2Crn2 (clay texture) and Ar (loamy fine sand), respectively.

diluting a certified standard solution (iron standard for ICP, TraceCERT®), and certified reference materials were used (NIST SRM 2709a) to ensure quality control. The sum of Py-Fe and Oxy-Fe was considered a pseudo-total Fe since these fractions represent the most important and active fractions in coastal wetland soils (Ferreira et al., 2007, 2022). Additionally, quantification of Py-Fe is a useful approach to improve the comprehension of Fe and sulfur dynamic in coastal wetland soils (for example, please see Queiroz et al., 2022; Jimenez et al., 2022; Ferreira et al., 2022). The degree of iron pyritization (DOP %) was calculated as follows: DOP (%) = Py-Fe/pseudo-total Fe (Berner, 1970). DOP values reflect the percentage of pseudo-total Fe incorporated into pyrite and enable comparisons among soils with different reactive Fe content (Berner, 1984, 1970).

Exchangeable bases (Na^+, K^+, Ca^{2+}, and Mg^{2+}) were extracted from salt-free samples with 1.0 mol L^{-1} ammonium acetate and determined by atomic absorption (Ca^{2+} and Mg^{2+}), atomic emission spectrometry (K^+), and flame photometry (Na^+). The exchangeable acidity (H + Al) was extracted with 1.0 mol L^{-1} KCl and determined by titration (IUSS Working Group, 2015; Van Reeuwijk, 2002). The sums of exchangeable bases ($\Sigma Na^+ + K^+ + Ca^{2+} + Mg^{2+}$), cation exchange capacity (CEC; CEC = sum of bases + $Al^{3+} + H^+$), exchangeable sodium percentage (ESP; ESP = $Na^+ \times 100/CEC$), and base saturation (base saturation: sum of bases $\times 100/CEC$) were calculated according to the IUSS Working Group WRB (2015).

Based on morphological, physical, and chemical analyses, all the soils were classified according to the FAO/WRB (IUSS Working Group WRB, 2015).

2.4 Mineralogical analysis

Samples from representative surface and subsurface horizons were chosen for mineralogical characterization. X-ray diffraction (XRD) analysis was carried out to identify the mineralogical assemblage of the sand and clay fractions. The sand fraction was separated using a 0.053 mm sieve after chemical dispersion with 0.015 mol L^{-1} $(NaPO_3)_6$ + 1.0 mol L^{-1} NaOH for 16 h shaking; silt and clay were separated according to Stoke's law.

The sand fraction was analyzed as randomly oriented powder mounts. The clay fraction was saturated with Mg^{2+} using 1 mol L^{-1} $MgCl_2$ solution. After saturation, the excess chloride was removed by several centrifugations using 95 % ethanol and distilled water. After ultrasonic dispersion, the saturated suspended clay was pipetted onto glass slides and dried overnight at room temperature to prepare oriented clay mounts. Clay samples were analyzed as follows: (1) Mg-saturated at room temperature (Mg), (2) Mg-saturated solvated with ethylene glycol (by exposure to a glycol-saturated atmosphere at 60 °C for 20 h; EG), and (3) Mg-saturated after heating at 550 °C for 2 h. X-ray diffraction patterns were obtained using a Rigaku Miniflex II with Cu-Kα radiation. The sand fraction was scanned from 3 to 50°2θ and the clay

fraction from 3 to 35°2θ, both with a 0.02°2θ s^{-1} step size and a count time of a 3 s^{-1} step.

2.5 Water analysis

The pH of all the water samples was immediately measured in the laboratory using a glass electrode calibrated with standard solutions (pH 4.0 and 7.0; Hanna HI 9025), whereas the salinity was determined using a hand refractometer. Water samples were then filtered (0.4 µm filter), acidified (nitric acid; pH < 2.0), and frozen for the determination of Ca^{2+} and Mg^{2+} using atomic absorption spectrophotometry, Na^{+} by flame photometry, Cl^{-} by titration, and sulfate by turbidimetry, according to the methods proposed by Nollet and De Gelder (2000).

2.6 Statistical analysis

Discriminant analysis (DA) was performed to develop a function that yielded optimal discrimination of the study sites (northeastern, southeastern, and southern coasts). DA allows the identification of the relative contribution of variables in separating the soil from biogeographical regions (Reimann et al., 2008). The relationships between variables were established using Spearman's rank correlation coefficient (r). All statistical tests were performed using XLSTAT version 2014.5.03 (copyright Addinsoft, USA).

3 Results

3.1 Morphological attributes

The studied soil profiles showed sequences of A–C horizons (along with eventual transitional AC or CA horizons) at different depths and with contrasting subordinate characteristics (i.e., horizon suffixes). The thickness of the surface A horizons ranged from 5 cm (SE2) to 12 cm (S2; Table 1). Soil profiles showed marked shifts in grain size composition, with lithologic discontinuities occurring at various depths (e.g., NE1 and NE2; Table 1). Some profiles also present discrete but intermingled horizons (e.g., 2Crn1/2Crn2 and Crn2/2Crn in S1 and S2, respectively). Soil colors varied widely between and within the studied profiles (Table 1). The studied soil horizons presented dominant soil matrix colors (e.g., NE2 and SE1; Table 1) and mottled soil color patterns (e.g., S1 and S2; Table 1) with different abundances, sizes, and depths. Soil horizons presented hues varying from yellowish (10Y) to purple bluish (5PB), with values between 2.5 and 6, chromas ranging from 0 to 8 (Table 1), and several horizons with neutral (i.e., chroma = 0; Table 1) and dark colors (i.e., low values, ranging from 2.5 to 5; chromas ranging from 0 to 2, e.g., N 2,5/ or 10Y 5/2; Table 1; Figs. 1, 2, and 3). Variegated colors and orange-reddish mottles were observed around the root channels in some studied soil profiles (Figs. 1, 2, and 3).

Soil textures also varied widely between and within soil profiles, showing textures from clay (e.g., S1, 2Crn2, 70 % of clay) to coarse sand (e.g., SE1, Arz, 5 % of clay; Table 1). Coarser soil textures were recorded on the southeastern coast, with sand contents ranging between 62 % and 89 % (mean 81.2 ± 7.2 %, Table 1) compared to the south (mean 68.5 ± 22.8 %, ranging from 11 to 91 %) and northeast (mean 64.5 ± 13.9 %, ranging from 44 % to 82 %). Regarding soil structure, soil horizons were apedal, showing both massive and single-grained grades, with single-grained structures recorded in horizons with coarser grain size composition (i.e., higher sand content, coarse sand or shell fragments; Table 1; Figs. 1, 2, and 3), whereas massive structures were recorded in horizons presenting loam to fine textures.

A higher abundance of roots was recorded in the northeastern and southern coastal soils, whereas roots were almost absent in the southeastern coastal soil profiles (Figs. 1 and 3). For the northeastern coastal soils, medium (diameter ranging from 2 to 5 mm) roots and rhizomes could be distinguished, whereas a predominance of very-fine (< 0.5 mm) and fine roots (0.5 to 2 mm) was recorded on the southern coast (Fig. 3). Additionally, intact and fragmented seashells were recorded in both the northeastern and southeastern coastal soils (Figs. 1 and 2), whereas none were recorded on the southern coast.

3.2 Soil physicochemical conditions

The pH_{field} values ranged from 6.77 to 7.84 between the soil profiles, indicating neutral to slightly alkaline conditions (Table 2). Higher mean pH_{field} values were observed in the south (7.51 ± 0.37), followed by the southeastern coast (7.35 ± 0.21), while lower values were recorded on the northeastern coast (6.99 ± 0.14). The $pH_{oxidation}$ values also differed significantly among the sites (Table 2). The lowest values ($pH_{oxidation}$ < 3.0) were recorded in the northeastern (mean $pH_{oxidation}$: 4.64 ± 1.73) and southern soils (mean $pH_{oxidation}$: 2.73 ± 0.39), whereas the highest $pH_{oxidation}$ values (> 5.0) were recorded in the southeastern soils (mean $pH_{oxidation}$: 6.02 ± 0.66; Table 2).

E_h varied widely among sites, ranging from −36 to +384 mV (Table 2). Redox conditions varied from anoxic (E_h < +100 mV) to oxic (E_h > +350 mV) in the northeastern and southern soils (values between −36 and +384 mV and between −36 and +366 mV for the northeastern and southern soils, respectively; Table 2). However, anoxic conditions prevailed (mostly in the surface horizons) in the northeast, whereas in the southern soils, redox conditions were anoxic in the lowermost horizons (Table 2). In contrast, suboxic (+100 mV < E_h < +350 mV) conditions predominated the southeastern soil profiles (values ranging between +113 and +304 mV). The studied soils also presented significant differences regarding EC, with higher values recorded in the northeastern soil profiles (mean 45.9 ± 3.8 dS m^{-1}),

Table 1. Morphological properties and grain size composition of subaqueous soils from Brazilian seagrass meadows.

Horizon	Depth (cm)	Matrix color	Color	Mottle[2]	Structure[3]	Plasticity[4]	Stickiness[5]	Sand	Silt (%)	Clay	Texture[6]	Boundary[7]
NE1 – Eutric Fluvic Reductigleyic Subaquatic Gleysol (Loamic, Hypersalic, Sodic, Hypersulfidic)												
Arz	0–10	5GY 3/1, 10YR 3/1[1]	Very dark greenish gray, very dark gray		MA	PL	SST	66	14	20	SCL/FSL	GS
CArz	10–26	5G 4/1	Dark greenish gray		MA	PL	SST	60	15	25	SCL	CS
Crz1	26–37	5GY 4/1	Dark greenish gray		MA	SPL	NST	78	6	16	FSL	AS
Crz2	37–56	10Y 4/1	Dark greenish gray		SG	NPL	NST	82	6	12	FSL	DS
2Crz	56–84	5GY 4/1	Dark greenish gray		SG	SPL	SST	80	2	18	FSL	CS
3Crnz	84–114+	10B 4/1	Dark bluish gray		MA	VPL	ST	48	12	40	SC	
NE2 – Eutric Fluvic Reductigleyic Subaquatic Gleysol (Loamic, Hypersalic, Sodic, Hyposulfidic)												
Arz	0–10	5GY 3/1	Very dark greenish gray		MA	PL	SST	62	18	20	SCL/FSL	CS
Crz	10–39	10Y 4/1	Dark greenish gray		SG	SPL	NST	80	3	17	FSL	AS
2Crz	39–47	5BG 3/1	Dark greenish gray		MA	PL	NST	61	14	25	SCL	CS
3Crnz1	47–91	5PB 4/1	Dark bluish gray		MA	VPL	SST	44	16	40	C/CL	DS
3Crz2	91–98+	5PB 4/1	Dark bluish gray		MA	VPL	ST	49	11	40	SC	
SE1 – Eutric Fluvic Reductigleyic Subaquatic Gleysol (Loamic, Hypersalic, Sodic, Hyposulfidic)												
Arz	0–6	10Y 3/2	Olive black		SG	SPL	NST	89	6	5	CS	CS
ACrz	6–11	10Y 4/1	Dark greenish gray		SG	SPL	NST	87	5	8	LCS	GS
2Crz1	11–17	10Y 3/1	Very dark greenish gray		SG	SPL	ST	82	6	13	CSL	CS
2Crz2	17–25	10Y 3/1	Very dark greenish gray		MA	NPL	NST	78	2	20	SCL/CSL	CS
2Crz3	25–34	10GY 2.5/1	Greenish black		SG	NPL	NST	82	5	12	FSL	CS
2Crz1	34–40	10GY 4/1	Dark greenish gray		SG	PL	NST	87	0	13	LCS	AI
3Crz2	40–48+	5G 5/1	Greenish gray		MA	PL	NST	71	7	22	SCL	
SE2 – Eutric Fluvic Reductigleyic Subaquatic Gleysol (Loamic, Hypersalic, Sodic, Hyposulfidic)												
Arz	0–5	10Y 5/2	Olive gray		SG	NPL	NST	87	3	10	LCS	CS
ACrz	5–12	10GY 3/1	Very dark greenish gray		SG	NPL	NST	86	4	10	LCS	GS
Crz	12–26	10GY 4/1	Dark greenish gray		SG	NPL	NST	86	1	13	CSL	GS
Crnz	26–33	10BG 3/1	Very dark greenish gray		MA	NPL	NST	81	4	15	CSL	CS
2Crz1	33–42	10BG 4/1	Dark greenish gray		MA	NPL	NST	80	3	17	CSL	CS
2Crz2	42–47	10B 3/1	Very dark bluish gray		SG	NPL	NST	82	0	18	CSL	CS
2Crz3	47–50+	10G 5/1, 10 YR 6/8[1]	Greenish gray, brown		MA	PL	NST	62	13	25	CSL	

followed by the southeastern (mean $39.8 \pm 3.5\,\mathrm{dS\,m^{-1}}$) and southern soils (mean $3.5 \pm 1.1\,\mathrm{dS\,m^{-1}}$; Table 2).

Soils from the northeastern coast presented the higher TOC contents (mean 2.5 ± 0.9 %, values ranging from 1.1 % to 3.5 %) when compared to soils on the southeastern (mean 0.4 ± 0.2 %, values ranging from 0.1 % to 0.6 %) and southern coasts (mean 0.6 ± 0.1 %, values ranging from 0.4 % to 0.8 %; Table 2). Additionally, on the northeastern coast, an increase in TOC content was observed in deeper soil layers (e.g., 3.2 % for both NE1 Crz2 at 37–56 cm depth and NE2 3Cmz1 at 47–91 cm depth), which was not observed for the other coastal compartments. Similarly, the higher CCE contents were also recorded at the northeastern coast (mean 7.0 ± 4.9 %), with values ranging from 2.0 % to 14.6 %, while the southeastern and southern coastal soils showed significantly lower CCE values (mean 1.9 ± 0.1 % and 1.8 ± 0.1 % to the southeastern and southern coasts, respectively; Table 3). As occurred with TOC contents, an increase in CCE content was observed in deeper soil horizons

Table 1. Continued.

Horizon	Depth (cm)	Matrix Color	Color	Mottle[2]	Structure[3]	Plasticity[4]	Stickiness[5]	Sand	Silt (%)	Clay	Texture[6]	Boundary[7]
S1 – Eutric Fluvic Reductigleyic Subaquatic Gleysol (Loamic, Protosalic, Sodic, Hypersulfidic)												
Ar	0–6	N 2.5/ 10Y 3/1[1]	Black, very dark greenish gray		SG	SPL	SST	85	5	10	LFS	CW
ACrj	6–13	2.5Y 5/1	Yellowish gray	7.5YR 4/4 CVD N 2.5/ VVD	SG	NPL	NST	91	4	5	FS	CW
CAr1	13–30	2.5Y 4/1	Yellowish gray		MA	SPL	SST	69	11	20	SCL/FSL	GS
CAr2	30–44	N 4/	Dark gray		MA	SPL	SST	80	4	16	FSL	GS
Cr	44–70	N 5/	Gray		SG	SPL	SST	81	4	15	FSL	GS
2Crn1	70–93	N 3/	Very dark gray		MA	PL	ST	50	20	30	SCL	CB
2Crn1/2Crn2	93–106	5B 3/1 N 3/ [1]	Very dark bluish gray, very dark gray		MA	PL	ST	80	5	15	FSL	CS
2Crn2	106–111	5B 3/1	Very dark bluish gray		MA	VPL	VST	26	4	70	C	
S2 – Eutric Fluvic Reductigleyic Subaquatic Gleysol (Loamic, Protosalic, Sodic, Hypersulfidic)												
Arj	0–12	2.5Y 5/1	Yellowish gray	7.5YR 4/4 VVD N 2.5/ VVD	SG	SPL	SST	85	5	10	LFS	CW
CAr1	12–25	2.5Y 4/1	Yellowish gray		MA	PL	ST	72	3	25	SCL	GS
CAr2	25–42	2.5Y 5/1	Yellowish gray		SG	SPL	SST	81	2	17	FSL	GS
Cr1	42–77	2.5Y 4/1	Yellowish gray		SG	SPL	SST	81	3	16	FSL	CS
Crn2	77–84	10B 4/1	Dark bluish gray		MA	SPL	SST	69	8	23	SCL	CS
Crn2/2Crn	84–94	10B 4/1	Dark bluish gray		MA	PL	ST	11	19	70	C	CS
2Cr	94–100	10B 6/1	Bluish gray		MA	VPL	VST	67	3	30	SCL	

[1] Variegated. [2] CVD: common, very fine, distinct. VVD: very few, very fine, distinct. [3] MA: massive. SG: single grain. [4] NPL: non-plastic. SPL: slightly plastic. PL: plastic. VPL: very plastic. [5] NST: non-sticky. SST: slightly sticky. ST: sticky. VST: very sticky. [6] C: clay. CL: clay loam. CS: coarse sand. CSL: coarse sandy loam. FSL: fine sandy loam. FS: fine sand. LCS: loamy coarse sand. LFS: loamy fine sand. SC: sandy clay. SCL: sandy clay loam. SL: sandy loam. [7] GS: gradual smooth. CS: clear smooth. AS: abrupt smooth. DS: diffuse smooth. CW: clear wavy. CB: clear broken (discontinuous).

from the northeastern profiles (e.g., 13.8 % and 12.8 % for both NE1 Crz2 and NE2 3Cmz1, respectively).

3.3 Iron partitioning and DOP

Iron partitioning and DOP showed marked differences among the sites. The northeastern soils showed higher contents of Py-Fe when compared to the other studied sites (Table 2); the mean contents of Py-Fe and Oxy-Fe were 70.9 ± 54.7 and $25.5 \pm 8.9\,\mu mol\,g^{-1}$, respectively. On the other hand, the southern coastal soils showed lower contents of Py-Fe (mean $45.4 \pm 42.1\,\mu mol\,g^{-1}$) and Oxy-Fe (mean $15.8 \pm 410.4\,\mu mol\,g^{-1}$). The southeastern coastal soils showed the highest contents of Oxy-Fe (mean $51.0 \pm 8.5\,\mu mol\,g^{-1}$), whereas the mean content of Py-Fe was $17.0 \pm 9.5\,\mu mol\,g^{-1}$ (Table 2). DOP values varied between 4 % and 84 % among the sites (Table 2). The higher DOP values were recorded in the northeast (65.5 ± 9.3 %) and the lower values in the southeastern coastal soils (23.9 ± 10.6 %; Table 2). In the south, the mean DOP value was 59.3 ± 24.5 % (Table 2).

3.4 Soil exchangeable cation capacity

The higher CEC values were recorded in the northeastern soils (mean $17.1 \pm 8.0\,cmol_c\,kg^{-1}$ ranging from 33.2 to $2.3\,cmol_c\,kg^{-1}$; Table 3), while lower values were found in the southern (mean $12.8 \pm 9.3\,cmol_c\,kg^{-1}$) and southeastern coastal soils (mean $11.5 \pm 2.9\,cmol_c\,kg^{-1}$). Despite CEC differences, the exchangeable complexes of the six representative soil profiles were mainly dominated by Ca^{2+} and Mg^{2+}, followed by Na^{+}. All the soil profiles showed high base saturation values (> 50 %; Table 3).

3.5 Mineralogy

The sand XRD diffractograms from both the surface and subsurface horizons of the northeastern and southern soils were dominated by quartz. Small peaks of biotite and feldspar were also recorded in the southeastern soils (Fig. 4a). The clay fraction XRDs highlighted the presence of smectite, illite, vermiculite, kaolinite, and different interstratified minerals (e.g., kaolinite–smectite and smectite–illite; Fig. 4b). Sharper kaolinite peaks were observed in the southern and northeastern coastal soils, whereas broader peaks were observed in the southeastern soils. In the northeast, peaks of smectite, smectite–illite, and illite were also observed (Fig. 4b), with sharper smectite and smectite–illite peaks at the surface layers. Vermiculite and goethite were only recorded on the southeastern coast (Fig. 4b) along with less intense kaolinite peaks (at the subsurface layers) and high intensities of the 2 : 1 clay peaks (smectite and vermiculite). On the southern coast, soils showed the presence of kaolin-

Table 2. Physicochemical conditions and Fe partitioning of seagrass meadow soils from the Brazilian coast.

Horizon	Depth	pH		E_h	EC	TOC	CCE	Oxy-Fe	Py-Fe	Pseudo-total Fe	DOP
	cm	field	Ox*	mV	dS m^{-1}	%		μmol g^{-1}			%
NE1 – Eutric Fluvic Reductigleyic Subaquatic Gleysol (Loamic, Hypersalic, Sodic, Hypersulfidic)											
Arz	0–10	6.78	4.92	−36	42	3.5	2.9	47.8	126.7	174.5	71
CArz	10–26	7.14	2.89	34	42	1.8	2.0	23.6	52.6	76.2	67
Crz1	26–37	7.06	2.76	4	45	1.2	2.3	14.3	44.7	59	66
Crz2	37–56	6.85	6.14	32	45	3.2	13.8	23.8	14.4	38.2	48
2Crz	56–84	6.88	6.96	222	45	2.9	14.6	31.3	152.0	183.3	75
3Crnz	84–114+	6.80	2.90	169	52	2.5	4.2	31.5	176.9	208.4	83
NE2 – Eutric Fluvic Reductigleyic Subaquatic Gleysol (Loamic, Hypersalic, Sodic, Hyposulfidic)											
Arz	0–10	6.89	5.26	−32	42	3.5	8.9	24.0	38.3	62.3	59
Crz	10–39	7.11	6.49	384	45	1.1	7.4	18.9	32.9	51.8	59
2Crz	39–47	7.12	2.70	294	45	1.9	2.2	24.3	66.7	91	69
3Crnz1	47–91	7.11	6.97	230	50	3.2	12.8	22.1	35.6	57.7	62
3Crz2	91–98+	7.10	3.04	169	52	2.9	5.9	19.4	39.5	58.9	62
SE1 – Eutric Fluvic Reductigleyic Subaquatic Gleysol (Loamic, Hypersalic, Sodic, Hyposulfidic)											
Arz	0–6	7.21	6.09	225	37	0.4	1.6	47.6	5.5	53.1	10
ACrz	06–11	7.24	5.49	212	37	0.5	1.9	57.0	7.5	64.5	11
2Crnz	11–17	7.35	5.00	128	42	0.6	1.8	53.5	24.1	77.6	30
2Crz1	17–25	7.25	5.24	113	43	0.5	1.8	52.2	27.4	79.6	34
2Crz2	25–34	7.10	6.52	162	36	0.4	1.9	51.6	27.1	78.7	34
2Crz1	34–40	7.42	6.96	219	40	0.3	2.1	34.1	13.5	47.6	34
3Crz2	40–48+	6.96	6.48	251	44	0.1	1.9	37.6	10.9	48.5	22
SE2 – Eutric Fluvic Reductigleyic Subaquatic Gleysol (Loamic, Hypersalic, Sodic, Hyposulfidic)											
Arz	0–5	7.63	6.64	239	37	0.2	1.9	50.5	5.6	56.1	10
ACrz	5–12	7.18	5.75	236	42	0.4	1.9	61.5	17.8	79.3	22
Crz	12–26	7.39	5.13	169	43	0.5	1.9	50.4	19.2	69.6	27
Crnz	26–33	7.38	5.21	132	36	0.4	2.0	55.0	33.7	88.7	37
2Crz1	33–42	7.50	6.45	210	34	0.2	1.9	45.3	26.0	71.3	36
2Crz2	42–47	7.70	6.66	304	42	0.2	1.8	66.8	14.7	81.5	18
2Crz3	47–50+	7.63	6.64	239	44	0.2	1.9	50.5	5.6	56.1	10
S1 – Eutric Fluvic Reductigleyic Subaquatic Gleysol (Loamic, Protosalic, Sodic, Hypersulfidic)											
Ar	0–6	7.72	2.99	269	3	0.6	1.9	13.2	0.7	13.9	5
ACrj	6–13	7.14	2.45	294	3	0.5	1.7	10.8	19.2	30	55
CAr1	13–30	6.98	2.28	366	2	0.6	1.7	16.1	53.1	69.2	76
CAr2	30–44	7.93	2.47	94	3	0.6	1.8	13.5	26.8	40.3	63
Cr	44–70	7.84	2.65	−36	4	0.6	1.7	10.5	16.5	27	60
2Crn	70–93	7.84	2.87	38	5	0.4	1.7	15.1	22.1	37.2	59
2Crn/2Crn2	93–106	7.73	3.30	39	4	0.5	1.8	15.2	16.9	32.1	45
2Crn2	106–111	7.58	2.83	40	2	0.8	1.8	49.0	24.2	73.2	66
S2 – Eutric Fluvic Reductigleyic Subaquatic Gleysol (Loamic, Protosalic, Sodic, Hypersulfidic)											
Arj	0–12	7.12	2.64	294	3	0.5	1.7	25.5	1.2	26.7	4
CAr1	12–25	6.77	2.28	274	3	0.7	1.6	16.0	56.2	72.2	69
CAr2	25–42	7.05	2.35	274	3	0.6	1.9	19.2	65.2	84.4	76
Cr1	42–77	7.81	2.49	246	5	0.8	1.8	6.8	56.7	63.5	74
Cr2	77–84	7.68	2.90	182	5	0.7	1.6	7.2	52.6	59.8	73
Crn2/2Crn	84–94	7.75	2.71	24	5	0.7	1.8	8.7	118.4	127.1	84
2Cr	94–100	7.66	3.77	40	2	0.5	1.9	10.9	150.8	161.7	80

Table 3. Exchangeable cations of seagrass meadow soils from the Brazilian coast.

Horizon	Depth	Na^+	K^+	Ca^{2+}	Mg^{2+}	Al^{3+}	H + Al	SB	Cation exchange capacity	Base saturation	Exchangeable sodium percentage
	cm	$cmol_c\ kg^{-1}$								%	
NE1 – Eutric Fluvic Reductigleyic Subaquatic Gleysol (Loamic, Hypersalic, Sodic, Hypersulfidic)											
Arz	0–10	0.3	0.6	8.3	1.7	< 0.01	3.4	10.9	14.3	76	2
CArz	10–26	0.1	0.3	1.8	2.6	< 0.01	2.8	4.8	7.6	63	1
Crz1	26–37	0.1	0.1	2.0	1.0	< 0.01	1.6	3.1	4.7	66	1
Crz2	37–56	0.1	0.2	7.2	2.4	< 0.01	0.4	9.9	10.3	96	1
2Crz	56–84	0.1	0.2	9.8	3.0	< 0.01	0.3	13.1	13.4	98	1
3Crnz	84–114+	3.2	2.1	9.7	7.5	< 0.01	1.5	22.5	24.0	94	13
NE2 – Eutric Fluvic Reductigleyic Subaquatic Gleysol (Loamic, Hypersalic, Sodic, Hyposulfidic)											
Arz	0-h10	0.5	0.9	13.7	9	< 0.01	3.3	24.1	27.44	99	2
Crz	10–39	0.3	0.3	9.9	3.5	< 0.01	0.1	14.0	14.13	99	2
2Crz	39–47	0.2	0.8	14	7.5	< 0.01	0.1	22.5	22.61	100	1
3Crnz1	47–91	4.1	2.3	10.6	9.5	< 0.01	0.2	26.5	26.67	99	15
3Crz2	91–98+	1	1.7	9.6	9	< 0.01	2.2	21.3	23.47	91	4
SE1 – Eutric Fluvic Reductigleyic Subaquatic Gleysol (Loamic, Hypersalic, Sodic, Hyposulfidic)											
Arz	0–6	0.9	0.4	6.8	2.0	< 0.01	0.4	10.1	10.5	96	9
ACrz	06–11	1.3	0.5	7.8	2.2	< 0.01	0.3	11.8	12.1	98	11
2Crnz	11–17	5.2	0.8	8.7	3.1	< 0.01	0.1	17.8	17.9	99	29
2Crz1	17–25	1.9	0.7	9.5	3.2	< 0.01	0.1	15.3	15.4	99	12
2Crz2	25–34	1.9	0.6	9.4	2.5	< 0.01	0.1	14.4	14.5	99	13
2Crz1	34–40	0.7	0.4	7.8	2.2	< 0.01	0.1	11.1	11.2	99	6
3Crz2	40–48+	0.6	0.5	2.3	3.4	< 0.01	0.1	6.8	6.9	99	9
SE2 – Eutric Fluvic Reductigleyic Subaquatic Gleysol (Loamic, Hypersalic, Sodic, Hyposulfidic)											
Arz	0–5	1.6	0.6	6.2	2.7	< 0.01	0.2	11.1	11.3	98	14
ACrz	5–12	1.1	0.5	5.7	2.7	< 0.01	0.4	10.0	10.4	96	11
Crz	12–26	1.3	0.6	5.8	2.4	< 0.01	0.1	10.1	10.2	99	13
Crnz	26–33	2.3	0.6	6.4	2.8	< 0.01	0.1	12.1	12.2	99	19
2Crz1	33–42	1.1	0.5	5.9	2.3	< 0.01	0.2	9.8	10.0	98	11
2Crz2	42–47	0.3	0.3	4.8	1.9	< 0.01	0.3	7.3	7.6	96	4
2Crz3	47–50+	1.6	0.6	6.2	2.7	< 0.01	0.2	11.1	11.3	98	14
S1 – Eutric Fluvic Reductigleyic Subaquatic Gleysol (Loamic, Protosalic, Sodic, Hypersulfidic)											
Ar	0–6	0.1	0.2	0.9	1.2	< 0.01	1.3	2.3	3.6	64	< 1
ACrj	6–13	0.1	0.1	0.4	0.9	< 0.01	0.9	1.4	2.3	61	1
CAr1	13–30	0.8	0.4	1.3	4.7	2.8	5	7.2	12.2	59	7
CAr2	30–44	0.5	0.4	0.9	2.8	1.7	3.9	4.6	8.5	54	6
Cr	44–70	0.1	0.3	0.5	1.7	1.1	2.2	2.6	4.8	54	2
2Crn	70–93	4.6	2.4	5.4	8.6	< 0.01	0.4	21.0	21.4	98	22
2Crn/2Crn2	93–106	4.5	2.7	6.2	8.4	< 0.01	0.1	21.8	21.9	99	22
2Crn2	106–111	4.4	2.7	9.3	10.1	< 0.01	0.2	26.5	26.7	99	16
S2 – Eutric Fluvic Reductigleyic Subaquatic Gleysol (Loamic, Protosalic, Sodic, Hypersulfidic)											
Arj	0–12	0.1	0.2	0.5	1	< 0.01	1.2	1.8	3.0	60	3
CAr1	12–25	1.3	0.5	1.6	5.3	3	7	8.7	15.7	55	8
CAr2	25–42	0.8	0.5	1	3.7	1.9	3.7	6.0	9.7	62	8
Cr1	42–77	0.6	0.3	0.8	2.6	1.2	2.8	4.3	7.1	60	8
Cr2	77–84	0.8	0.9	2.9	3.8	< 0.01	1.1	8.4	9.5	88	8
Crn2/2Crn	84–94	4.9	4.0	10.4	13.8	< 0.01	0.1	33.1	33.2	100	15
2Cr	94–100	1.2	1.2	4.3	5.1	< 0.01	0.4	11.8	12.2	97	10

ite, smectite, smectite–illite, and illite, with sharper peaks on the soil surface (Fig. 4b).

3.6 Discriminant analysis

Discriminant analysis showed clear differentiation among soils from different coasts (Fig. 5). Function 1, with a total variance of 91.89 %, allowed discrimination of northeastern and southeastern soils from those of the southern coast, primarily based on salinity (eigenvector: −0.005), SO_4^{2-} (eigenvector: −0.001), EC (eigenvector: −0.073), $pH_{oxidation}$ (eigenvector: −0.116), Oxy-Fe (eigenvector: −0.011), and pH_{field} (eigenvector: −0.148). Function 2, with a total variance of 8.11 %, was correlated with TOC (eigenvector: 0.354), DOP (eigenvector: −0.002), CCE (eigenvector: 0.002), Py-Fe (eigenvector: 0.001), and ESP (eigenvector: −0.025) and allowed the discrimination of northeastern soils from those on the southeastern and southern coasts (Fig. 5). Soils from the northeastern coast were associated with higher TOC, CCE, CEC, and EC contents. In contrast, soils from the southern coast were associated with lower EC and $pH_{oxidation}$. Soils from the southeastern coast were associated with lower DOP values and higher Oxy-Fe and $pH_{oxidation}$ values (Fig. 5).

3.7 Soil classification

Based on the presented data (morphological, physical, and chemical), the six studied soils were classified as Eutric Fluvic Reductigleyic Subaquatic Gleysols according to the FAO/WRB soil classification; however, there were marked differences in their subqualifiers (Table 1).

Soils showed clear differences in EC, ESP, sulfide content (i.e., Py-Fe), and the capacity to generate intense acidification upon oxidation (i.e., the presence of hypersulfidic material). The NE1 profile met the criteria for hypersalic ($EC > 30\,dS\,m^{-1}$), sodic (saturation of $Na^+ + Mg^{2+} > 15\,\%$ and $ESP > 6\,\%$), and hypersulfidic ($pH_{oxidation} < 2.5$); thus, it was classified as Eutric Fluvic Reductigleyic Subaquatic Gleysol (Loamic, Hypersalic, Sodic, Hypersulfidic). On the other hand, both southeastern soils (SE1 and SE2) were classified as Eutric Fluvic Reductigleyic Subaquatic Gleysols (Loamic, Hypersalic, Sodic, and Hyposulfidic) because they did not meet the criteria for hypersulfidic material.

Hypersulfidic material and sodic horizons were identified in the southern soils (S1 and S2). However, the lower electrical conductivity ($< 15\,dS\,m^{-1}$) met the criteria for a protosalic qualifier ($EC > 4\,dS\,m^{-1}$). Thus, soils from the southern coast were classified as Eutric Fluvic Reductigleyic Subaquatic Gleysol (Loamic, Protosalic, Sodic, and Hypersulfidic).

3.8 Water analysis

Water chemistry and salinity showed significant differences between the coastal compartments (Table 4). Higher salinities were recorded on the northeastern coast (> 40; Table 4) along with higher concentrations of cations and anions, especially $Cl^- \gg Na^+ \gg SO_4^{2-} \sim Mg^{2+} > Ca^{2+}$ (Table 4). Conversely, cations, anions, and salinity were slightly lower on the southeastern coast, whereas the lowest salinities and concentrations of cations and anions were recorded on the southern coast (Table 4).

4 Discussion

4.1 Effects of the geological and bioclimatic settings on the geochemical pedoenvironments

Although the studied soils presented a dominance of sand (approximately 50 %; Table 1), the contrasting geological (i.e., sedimentary and igneous/metamorphic rocks) and hydrodynamic settings between the studied sites caused different degrees of sand deposition by the size-sorting mechanism (preferential removal of fine particles; Mueller et al., 2008). The finer texture of the northeastern (Table 1) soils is likely related to the lower river discharges in the estuaries owing to the semiarid climate conditions of the region (lower annual rainfall and high evapotranspiration rates; Alvares et al., 2013) and to the higher vegetation density (Fig. S1), which favors the trapping of fine particles (Larcombe et al., 2001). Additional deposition of allochthonous material (both mineral and organic; see Inoue et al., 2011) is significantly enhanced by the presence of high-density vegetation (Mazarrasa et al., 2015) and is favored by larger seagrass species or by those with greater biomass (Mazarrasa et al., 2015). Moreover, the occurrence of finer-textured soil horizons interspersed with (or followed by) coarse-textured horizons indicates a variation in hydrodynamic energy, which also indicates different depositional processes (Schoeneberger et al., 2002) where coarser textures are associated with higher-energy depositional events (Flemming, 2000). These processes are likely responsible for the presence of lithological discontinuities in all the soil profiles (Table 1). Moreover, the higher TOC contents observed in deeper soil horizons from the northeastern coast may indicate that these subaqueous soils resulted from successive depositional events burrowing former A horizons.

The marked differences in the geological and hydrological settings of the studied sites also resulted in differences in the mineralogical compositions of the soil profiles (Fig. 4a). In the northeastern and southern soils, the sand fraction presented a poor Fe monomineralic assemblage predominantly composed of quartz, likely due to inputs from the surrounding Cenozoic sandy deposits, that is, Barreiras tablelands and Quaternary plains, respectively (Campos et al., 2008; Dominguez, 2006). However, on the southeastern coast, the

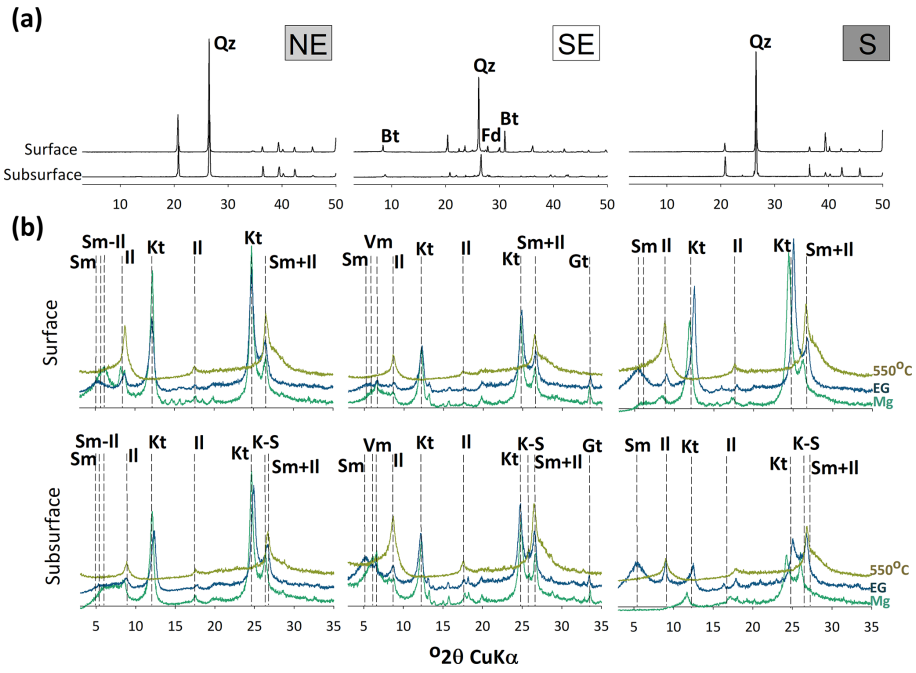

Figure 4. XRD patterns of sand **(a)** and clay fractions **(b)** from the seagrass soils of the different studied coastal compartments (northeastern – NE; southeastern – SE; southern – S). Bt: biotite; Fd: feldspar; Il: illite; Kt: kaolinite; K–S: kaolinite–smectite; Qz: quartz; Sm: smectite; Sm-Il: smectite–illite; Vm: vermiculite.

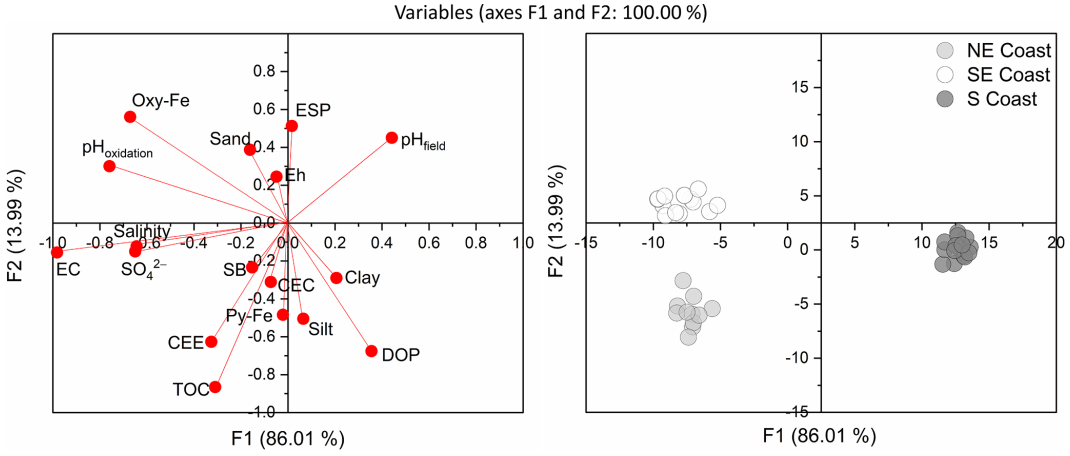

Figure 5. Discriminant analysis (DA) showing the differentiation of the seagrass soils from the three studied coastal compartments (northeastern coast, southeastern coast, and southern coast). CCE: calcium carbonate equivalent; CEC: cation exchange capacity; EC: electrical conductivity; ESP: exchangeable sodium percentage; Oxy-Fe: Fe oxyhydroxides; Py-Fe: pyritic Fe; TOC: total organic carbon.

granitic gneiss outcrops of the Serra do Mar act as sources of both biotite and feldspars in the estuary (Souza-Júnior et al., 2007).

Clay mineralogy also reflects contrasting geological settings (Fig. 4b). The Barreiras Formation, on the northeastern coast, and the Quaternary deposits on the southern coast, mainly composed of kaolinite and illite (Albuquerque et al., 2014; Lopes et al., 2016; Melo et al., 2002), directly influence the clay mineralogy of the seagrass soils. Despite the predominance of sand, the northeastern soils presented high-activity clays (mostly smectite, illite, and interstratified mineral species), which indicates an active mineral transformation process (Środoń, 1999). These minerals are likely formed owing to the high ionic force commonly found in intertidal and marine environments (Furquim et al., 2008; Velde and Church, 1999), which is corroborated by the high ion concentrations in the estuarine water from the northeastern coast (Table 4). Such mineralogical transformations may

Table 4. Average values ($n = 3 \pm$ standard deviation) of the physicochemical parameters (pH, salinity, cations, and anion concentration) of the water column from the three coastal compartments (northeastern, southeastern, and southern Brazilian coast).

Site	pH	Salinity	Ca^{2+}	Mg^{2+}	Cl^-	Na^+	K^+	SO_4^{2-}
			$mg\,L^{-1}$					
Northeastern coast	8.6 ± 0.2	42 ± 0	467 ± 21	1460 ± 131	$18\,550 \pm 353$	$11\,317 \pm 1279$	253 ± 104	1168 ± 44
Southeastern coast	8.5 ± 0.1	39 ± 3	474 ± 21	1281 ± 77	$17\,500 \pm 459$	9767 ± 189	333 ± 15	1021 ± 38
Southern coast	8.1 ± 0.1	5 ± 0	9 ± 4	20 ± 7	455 ± 15	233 ± 50	13 ± 2	43 ± 11

also be inferred by the decrease in the intensity of the kaolinite peaks along with the enlargement of 2 : 1 peaks with depth (i.e., subsurface horizons, Fig. 4; Andrade et al., 2014). On the other hand, on the southeastern coast, the weathering of Fe-containing minerals (e.g., biotite; Fig. 4) sourced from the Serra do Mar outcrops favors the formation of Fe oxides and their deposition in the estuary (Ferreira et al., 2022). The peaks of goethite (Fig. 4) registered in these soil compartments are also likely related to the weathering of Fe-bearing primary minerals in the surrounding watershed soils (Souza-Júnior et al., 2008). Additionally, the higher Oxy-Fe contents in the southeastern coastal soils (Table 2) corroborate a more efficient source of Fe in this geological setting (Ferreira et al., 2022).

The differences in the physical and mineralogical compositions of the studied soils seemed to affect the TOC content (Table 2). In the northeastern coastal soils, the significantly higher TOC contents (mean 2.5 ± 0.1 %) were associated with higher plant biomass (Fig. 1) but also with the higher clay contents and 2 : 1 clay mineralogy. This suggests the presence of organic–mineral interactions as a driver of organic matter persistence (Lehmann and Kleber, 2015). Under such conditions, the higher CEC (Table 3) of 2 : 1 clays (Fig. 4) and the high concentrations of divalent cations (i.e., Ca^{2+} and Mg^{2+}; Table 3) would favor the formation of organic–mineral complexes (Kida et al., 2017), promoting organic matter stabilization and preventing its decomposition (Schmidt et al., 2011). The positive and significant correlations between TOC and cation exchange capacity (TOC vs. CEC; $r = 0.415$; $p < 0.01$; see Supplement) and exchangeable $Ca^{2+} + Mg^{2+}$ (TOC vs. $Ca^{2+} + Mg^{2+}$; $r = 0.466$; $p = 0.002$; see Supplement) corroborate this stabilization mechanism.

The differences in the physicochemical parameters of the water column (Table 4) also revealed the effects of contrasting geological and hydrological settings among the studied sites. The significantly lower EC values and ionic concentrations at the southern coast are both related to sandy materials in the geological surroundings and the geomorphological features of the estuary. The latter is characterized by a choked lagoon where seawater influx is limited (Seeliger, 2001). Conversely, the higher salinities and ionic concentrations found on the northeastern coast (Tables 2 and 4) are related to the low freshwater input in these estuaries because of the dominant semiarid climate in the region's watersheds (Lacerda et al., 2007).

4.2 Contrasting geochemical conditions and their effects on soil-forming processes

The different geological, bioclimatic, and hydrodynamic settings of the Brazilian coast produced contrasting geochemical pedoenvironments, which caused different intensities of pedogenetic processes and, ultimately, soil diversity among the studied sites.

Because of the abundant sulfate supply from seawater, hydromorphic conditions, organic matter inputs from vegetation, and deposition of reactive Fe from hydrological systems (i.e., rivers and tides), Fe and S bacterial reductions are the main pathways of respiration in these ecosystems (Nóbrega et al., 2013; Holmer et al., 2001; Brodersen et al., 2017; Giblin, 1988) (Reactions 1 and 2; Canfield et al., 1993). Thus, the geochemical environment to which the studied soils were subject is prone to both *gleization* and *sulfidization* (Schaetzl and Thompson, 2015; Ferreira et al., 2007), which are processes typically active in hydric soils (Veneman et al., 2015; Lowry et al., 2012; Ferronato et al., 2016). However, the intensity and reach of such processes varied widely among the studied sites and, thus, ultimately produced diverse soils depending on the characteristics of each pedoenvironment.

Although gleization-related colors occurred in all studied profiles (i.e., dark greenish-bluish soil colors with low values and chromas, e.g., N2.5–5/, 5BG 3/1, 5PB4/1; Figs. 2 and 3; Table 1), our data showed varying intensities of gleization, which are related to the (seemingly subtle) differences in the geochemical environment of each study site. Upon gleization, solid Fe(III) forms (oxyhydroxides and oxides) are reduced (and solubilized; Reaction 1), leading to the formation of Fe(II), which can either be removed from the soil (Otero et al., 2008) or reprecipitated as poorly crystalline Fe oxyhydroxides (Reaction 2; Canfield et al., 1993), forming high chroma mottles (e.g., along the root and benthos burrows; Figs. 1, 2, and 3), which contrasts with the surrounding soil matrix dominated by lower chromas and gray hues (Figs. 1, 2, and 3). Within the studied seagrass soils, roots showed a marked influence on gleization and affected soil morphology by creating variegated soil colors and brown mottles (especially in the upper soil horizons of some profiles; Fig. 3; Ta-

ble 1). These variegated colors result from the oxidation of dissolved Fe^{2+} (Reaction 2) promoted by the rhizospheres of these marine phanerogams (Weiss et al., 2004).

$$FeOOH + 3H^+ + e^- \rightarrow Fe^{2+} + 2H_2O \quad (R1)$$

$$4Fe^{2+} + O_2 + 6H_2O \rightarrow 4FeOOH + 8H^+ \quad (R2)$$

As Fe oxyhydroxides are solubilized, the soil matrix acquires bluish/greenish dark gray colors (e.g., 5BG 3/1, 10BG 4/1, and 10BG 3/1; Table 1), which also reflects the presence of Fe-rich clays (e.g., glauconite and nontronite) (Prada-Gamero et al., 2004; Souza-Júnior et al., 2008; Pugliese Andrade et al., 2014). The presence of such clays results from mineral transformations triggered by the high Fe activity (from Fe-oxyhydroxide dissolution) and high salinities (Pugliese Andrade et al., 2014; Souza-Júnior et al., 2010).

However, on the southeastern coast, gleization was less intense than that in the northeastern and southern coastal soils. The significantly higher contents of Oxy-Fe in the southeastern soils ($51.0 \pm 8.5\ \mu mol\ g^{-1}$; Table 2) show the less intense gleization (i.e., Fe-reduction) process. The higher E_h values ($+203 \pm 55$ mV; Table 2) and significantly lower TOC contents (0.4 ± 0.2 %; Table 2) when compared to soils from other coastal compartments characterized a geochemical environment less prone to the reduction of Fe oxyhydroxides (see Fig. 6). Additionally, the presence of goethite XRD peaks (Fig. 4b), only observed in the southeastern soils, further corroborates the lower intensity of gleization at this site as well as the direction of the Oxy-Fe vector towards the plotted data of the southeastern coast in the DA (Fig. 5). In this case, the goethite that is transported as suspended sediments (Souza-Júnior et al., 2008) settles within seagrass meadows and is preserved as a result of the prevailing redox conditions caused by the low TOC contents for microbial metabolism (Søndergaard, 2009).

As organic matter decomposition proceeds and most of the ferric-Fe compounds are consumed, bacteria start using sulfate from seawater as the terminal electron acceptor, producing sulfides (Reaction 3; Canfield et al., 1993; Nóbrega et al., 2016). Since ferrous Fe is generally present, the precipitate of different Fe sulfides (e.g., pyrite and/other metastable phases such as the "acid volatile sulfides", i.e., greigite and mackinawite; Reactions 4 and 5) produces dark-colored spots (like those observed in the subsurface horizons of the northeastern soil profiles; Fig. 1) characteristic of the sulfidization process, e.g., 5PB 4/1, 10B 3/1, and 10B 4/1 (Macías and Camps-Arbestain, 2020; Otero et al., 2008).

Sulfidization was also evidenced by the accumulation of sulfidic material ($pH_{oxidation} \leq 2.5$; Table 2) and by the DOP values (> 50 %; Table 2) registered in all the studied soil profiles; the significant negative correlation between both proxies corroborates this statement ($r = -0.518$; $p < 0.01$; $n = 40$; see Fig. S3). On the other hand, the significantly higher DOP values found in the northeastern soils (65.5 ± 9.3 %; Table 2) suggest a greater intensity of sulfidization in this coastal region. In this case, the higher TOC contents (2.5 ± 0.9 %; Table 2) fueled by the high plant densities and biomass (see the Supplement) favor a more reduced geochemical environment and, ultimately, sulfate reduction (Fig. 6). Indeed, the soil profiles from the northeastern coast showed 6-fold and 2-fold higher Py-Fe contents ($70.9 \pm 54.7\ \mu mol\ g^{-1}$) than the southeastern and southern coastal soils, respectively (Table 2). Notably, despite the high Py-Fe contents in the northeastern soils (Table 2), the higher CCE ($7.00 \pm 0.48\ cmol_c\ kg^{-1}$; Table 2) and the presence of biogenic seashells (Fig. 1g–h) prevented the acidification in some soil horizons (Crz and 2Crz from soil profile NE1 and Crz and 3Crz from profile NE2), resulting in circumneutral $pH_{oxidation}$ values (Table 2). This natural buffering capacity highlights the importance of biogenic calcium carbonates in hampering soil acidification (Payne and Stolt, 2017; Still and Stolt, 2015; Vittori Antisari et al., 2016).

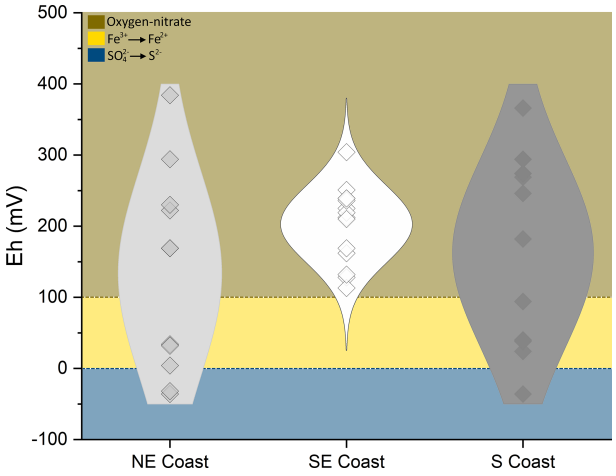

Figure 6. E_h values registered in the studied soil profiles. The shaded areas indicate the E_h intervals indicative of oxygen, nitrate (< +100 mV; brown area), Fe (+100–0 mV; yellow area), and SO_4^{2-} reductions (blue area) at a pH close to 7.0 (Søndergaard, 2009).

$$SO_4^{2-} + 9H^+ 8e^- \rightarrow HS^- + 4H_2O \quad (R3)$$

$$2Fe^{2+} + 2HS^- \rightarrow 2FeS + H_2 \quad (R4)$$

$$2Fe^{2+} + 4HS^- \rightarrow 2FeS_2 + 2H_2 \quad (R5)$$

The higher TOC contents in the seagrass soils located on the northeastern coast are especially relevant because they are consistently higher than those previously recorded for the surrounding semiarid terrestrial soils (mean 0.6 ± 0.1 %) and humid forest soils (mean 1.1 ± 0.3 %; Nóbrega et al., 2019).

Seagrass meadows have been globally recognized as significant carbon sinks, with most C sequestered within their soils (Serrano et al., 2016a, b). When compared to global data (mean 1.8 ± 0.3 % and median 1.2 % according to Fourqurean et al., 2012, or mean 2.5 ± 0.1 % and median 1.8 % according to Kennedy et al., 2010), the C contents

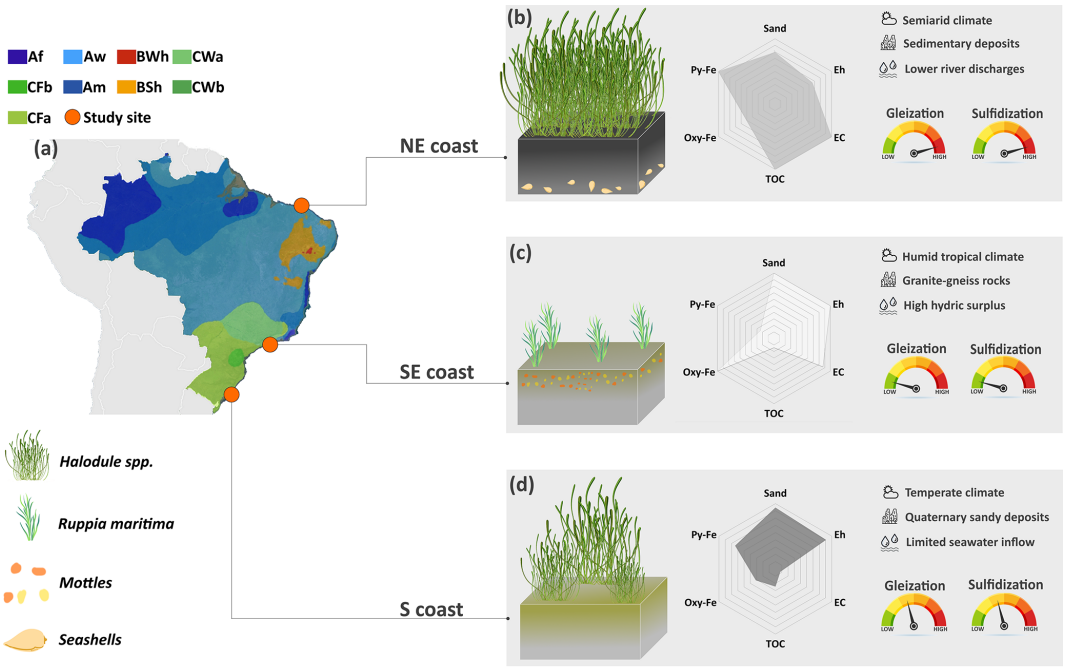

Figure 7. Graphical abstract illustrating the control exerted by the contrasting environmental (i.e., geological, hydrological, and bioclimatic) settings along the Brazilian coast over the geochemical pedoenvironments and its consequences for the intensities of soil-forming processes (i.e., gleization and sulfidization). On the northeastern coast, the denser plant coverage favored higher TOC contents and an anaerobic environment prone to more intense sulfidization. The lower river discharges in the northeast, due to the semiarid climate conditions, produced soils with finer textures and high-activity clays, more efficient in stabilizing soil organic matter. In the southeast, the sparse vegetation favors soils with lower TOC contents and also the establishment of a less oxidizing (i.e., suboxic) environment. Additionally, the Fe-rich geological surroundings constitute a more efficient source of Fe to the estuary decreasing the intensity of gleization. At the S, the geological surroundings marked by Quaternary Fe-poor sandy deposits, along with the geomorphological feature of the estuary (i.e., a choked lagoon), significantly lower the EC and ionic concentrations (especially sulfate) and ultimately decrease both the intensities of gleization and sulfidization.

of the studied seagrass soils were considerably lower (mean 1.0 ± 1.0 % and median 0.6 % for all the studied sites), except for those observed on the northeastern coast (mean 2.5 ± 0.1 %). Thus, seagrass meadows may constitute a relevant (but not yet quantified) C sink in the tropics, indicating that efforts in seagrass replanting and restoration should be considered for climate mitigation. However, the TOC content was highly variable among the studied soils from the different compartments (Table 2). These data reinforce the need to obtain local- and regional-scale inventories to better understand and quantify the role of tropical seagrass soils as sinks for C.

Additionally, it is worth noting that gleization and sulfidization are both controlled by the availability of metabolizable organic matter that stimulates dissolved oxygen consumption, followed by the metabolic pathways of Fe oxyhydroxides and sulfate reduction. Therefore, our results demonstrate not only the variability of these soils for carbon storage, but also how soil-forming processes can vary considerably in response to different environmental settings.

5 Conclusions

Despite some similarities among the studied subaqueous soils, the unique environmental features that characterize the different biogeographical regions of the Brazilian coastline (e.g., water column characteristics, geological setting, and varying hydrodynamics) result in different intensities of pedogenetic processes (Fig. 7). The characteristics of Brazilian seagrass soils reflect the effects of hydrological, geological, and bioclimatic settings on pedogenesis, which results in different intensities of gleying and sulfidization processes and, ultimately, in the relevant pedodiversity (Fig. 7). Additionally, the different intensities of these pedogenetic processes may affect the capacity of seagrass meadows to provide important ecosystem services (e.g., carbon sequestration).

The contrasting pedogenesis observed in the studied tropical seagrass meadows is a valuable contribution to the knowledge of these poorly studied (especially from a pedological perspective) and ecologically valuable tropical ecosystems. The overall findings of the present study are useful not only for a better understanding of the general functioning of seagrass meadows, but also for fostering environmental studies

focused on ecosystem service conservation and sustainable management of these meadows within the tropics.

Data availability. Data will be available upon reasonable request.

Supplement. The supplement related to this article is available online at: https://doi.org/10.5194/soil-9-189-2023-supplement.

Author contributions. GNN: first author writing the original and review articles, fieldwork, acquisition of the financial support, conceptualization of ideas, validation, formal analysis, and data curation. XLO: acquisition of the financial support, conceptualization of ideas. Provision of study materials, reagents, materials, and instrumentation. Writing and critical reviews. DJR: conceptualization, writing, reviewing, and editing, critical review data curation, validation, and formal analysis. HMQ: writing, reviewing, and editing, data curation, funding acquisition, validation, and formal analysis. DG: conceptualization, writing, reviewing, and editing, data curation, formal analysis, funding acquisition, and validation. MdSC: writing, reviewing, and editing, data curation, formal analysis, and resources. MdCP: writing, reviewing, and editing, data curation, and formal analysis. TOF: acquisition of the financial support, conceptualization of ideas, and formulation and evolution of research goals. Provision of study materials, reagents, materials, and instrumentation. Writing and critical reviews. Supervision and project administration.

Competing interests. The contact author has declared that none of the authors has any competing interests.

Disclaimer. Publisher's note: Copernicus Publications remains neutral with regard to jurisdictional claims in published maps and institutional affiliations.

Acknowledgements. The authors are thankful for the financial support received from the Fundação de Amparo à Pesquisa do Estado de São Paulo (FAPESP) (grant no. GNN: 2014/11778-5; HMQ: 2021/00221-3; TOF: 2016/21016-6; 2019/19987-6), Fundação Carlos Chagas Filho de Amparo à Pesquisa do Estado do Rio de Janeiro (GNN: grant no. E-26/202.757/2019), Programa Cientista Chefe do Meio Ambiente (FUNCAP), Conselho Nacional de Desenvolvimento Científico e Tecnológico (CNPq, grant nos. 305996/2018-5 and 409593/2018-4), Coordenação de Aperfeiçoamento de Pessoal de Nível Superior – Brasil (CAPES) – Finance Code 001, Consellería de Educación, Universidade e Formación Profesional-Xunta de Galicia (Axudas á consolidación e estruturación de unidades de investigación competitivas do SUG del Plan Galego IDT, Ambiosol Group, ref. 2018-PG036), CSIRO Oceans, and the Atmosphere–Coasts Program. Field sampling in South Brazil was supported by the Brazilian Long-Term Ecological Research (BR-LTER) – Site 8 – Patos Lagoon Estuary and the adjacent marine region. We are also very grateful for the logistical and human support provided by the Laboratory of Geological Oceanography (LOG) from the Federal University of Rio Grande (FURG).

Financial support. This research has been supported by the Fundação de Amparo à Pesquisa do Estado de São Paulo (grant nos. 2014/11778-5, 2021/00221-3, 2016/21016-6, and 2019/19987-6), the Fundação Carlos Chagas Filho de Amparo à Pesquisa do Estado do Rio de Janeiro (grant no. E-26/202.757/2019), the Conselho Nacional de Desenvolvimento Científico e Tecnológico (grant nos. 305996/2018-5 and 409593/2018-4), the Coordenação de Aperfeiçoamento de Pessoal de Nível Superior (Finance Code 001), FUNCAP research fellow (Chief Scientist Program), and the Consellería de Cultura, Educación e Ordenación Universitaria, Xunta de Galicia (grant no. 2018-PG036).

Review statement. This paper was edited by Claudio Zaccone and reviewed by Vanessa Wong and Livia Vittori Antisari.

References

Albuquerque, A. G. B. M., Ferreira, T. O., Nóbrega, G. N., Romero, R. E., Júnior, V. S. S. S., Meireles, A. J. A. A., and Otero, X. L.: Soil genesis on hypersaline tidal flats (apicum ecosystem) in a tropical semiarid estuary (Ceará, Brazil), Soil Res., 52, 140, https://doi.org/10.1071/SR13179, 2014.

Alvares, C. A., Stape, J. L., Sentelhas, P. C., De Moraes Gonçalves, J. L., and Sparovek, G.: Köppen's climate classification map for Brazil, Meteorol. Z., 22, 711–728, https://doi.org/10.1127/0941-2948/2013/0507, 2013.

Banco de dados climáticos do Brasil: https://www.cnpm.embrapa.br/projetos/bdclima/index.html, last access: 26 August 2019.

Baden, S., Emanuelsson, A., Pihl, L., Svensson, C., and Åberg, P.: Shift in seagrass food web structure over decades is linked to overfishing, Mar. Ecol. Prog. Ser., 451, 61–73, https://doi.org/10.3354/meps09585, 2012.

Berner, R. A.: Sedimentary pyrite formation: An update, Geochim. Cosmochim. Ac., 48, 605–615, https://doi.org/10.1016/0016-7037(84)90089-9, 1984.

Berner, R. A.: Sedimentary pyrite formation, Am. J. Sci., 268, 1–23, https://doi.org/10.2475/ajs.268.1.1, 1970.

Bezerra, C. E. E., Ferreira, T. O., Romero, R. E., Mota, J. C. A., Vieira, J. M., Duarte, L. R. S., and Cooper, M.: Genesis of cohesive soil horizons from north-east Brazil: Role of argilluviation and sorting of sand, Soil Res., 53, 43–55, https://doi.org/10.1071/SR13188, 2015.

Bower, C. A., Reitemeier, R. F., and Fireman, M.: Exchangeable cation analysis of saline and alkali soilS, Soil Sci., 73, 251–262, https://doi.org/10.1097/00010694-195204000-00001, 1952.

Bradley, M. P. and Stolt, M. H.: Subaqueous Soil-Landscape Relationships in a Rhode Island Estuary, Soil Sci. Soc. Am. J., 67, 1487–1495, https://doi.org/10.2136/sssaj2003.1487, 2003.

Bradley, M. P. and Stolt, M. H.: Landscape-level seagrass–sediment relations in a coastal lagoon, Aquat. Bot., 84, 121–128, https://doi.org/10.1016/j.aquabot.2005.08.003, 2006.

Brodersen, K. E., Koren, K., Moßhammer, M., Ralph, P. J., Kühl, M., and Santner, J.: Seagrass-Mediated Phosphorus and Iron Sol-

ubilization in Tropical Sediments, Environ. Sci. Technol., 51, 14155–14163, https://doi.org/10.1021/acs.est.7b03878, 2017.

Campos, E. J. D., Mulkherjee, S., Piola, A. R., and de Carvalho, F. M. S.: A note on a mineralogical analysis of the sediments associated with the Plata River and Patos Lagoon outflows, Cont. Shelf Res., 28, 1687–1691, https://doi.org/10.1016/j.csr.2008.03.014, 2008.

Canfield, D. E., Thamdrup, B., and Hansen, J. W.: The anaerobic degradation of organic matter in Danish coastal sediments: Iron reduction, manganese reduction, and sulfate reduction, Geochim. Cosmochim. Ac., 57, 3867–3883, https://doi.org/10.1016/0016-7037(93)90340-3, 1993.

Christian, R. R. and Luczkovich, J. J.: Organizing and understanding a winter's seagrass foodweb network through effective trophic levels, Ecol. Modell., 117, 99–124, https://doi.org/10.1016/S0304-3800(99)00022-8, 1999.

Copertino, M. S., Creed, J. C., Lanari, M. O., Magalhães, K., Barros, K., Lana, P. C., Sordo, L., and Horta, P. A.: Seagrass and Submerged Aquatic Vegetation (VAS) Habitats off the Coast of Brazil: state of knowledge, conservation and main threats, Brazilian J. Oceanogr., 64, 53–80, https://doi.org/10.1590/S1679-875920161036064sp2, 2016.

Costanza, R., de Groot, R., Sutton, P., van der Ploeg, S., Anderson, S. J., Kubiszewski, I., Farber, S., and Turner, R. K.: Changes in the global value of ecosystem services, Glob. Environ. Chang., 26, 152–158, https://doi.org/10.1016/j.gloenvcha.2014.04.002, 2014.

Copertino, M.: Add coastal vegetation to the climate critical list, Nature, 473, 255–255, https://doi.org/10.1038/473255a, 2011.

Demas, G. P.: Submerged Soils: A New Frontier in Soil Survey, Soil Horizons, 34, 44, https://doi.org/10.2136/sh1993.2.0044, 1993.

Demas, G. P., Rabenhorst, M. C., and Stevenson, J. C.: Subaqueous Soils: A Pedological Approach to the Study of Shallow-Water Habitats, 19, 229, https://doi.org/10.2307/1352228, 1996.

Dominguez, J. M. L.: The Coastal Zone of Brazil: an Overview, J. Coast. Res., 1, 16–20, 2006.

Duarte, C. M. and Chiscano, C. L.: Seagrass biomass and production: a reassessment, Aquat. Bot., 65, 159–174, https://doi.org/10.1016/S0304-3770(99)00038-8, 1999.

Duarte, C. M., Middelburg, J. J., and Caraco, N.: Major role of marine vegetation on the oceanic carbon cycle, Biogeosciences, 2, 1–8, https://doi.org/10.5194/bg-2-1-2005, 2005.

Duarte, C. M., Marbà, N., Gacia, E., Fourqurean, J. W., Beggins, J., Barrón, C., and Apostolaki, E. T.: Seagrass community metabolism: Assessing the carbon sink capacity of seagrass meadows, Global Biogeochem. Cy., 24, GB4032,, https://doi.org/10.1029/2010GB003793, 2010.

Erich, E. and Drohan, P. J.: Genesis of freshwater subaqueous soils following flooding of a subaerial landscape, Geoderma, 179, 53–62, https://doi.org/10.1016/j.geoderma.2012.02.004, 2012.

FAO: Standard operating procedure for soil calcium carbonate equivalent, Titrimetric method, Rome, https://www.fao.org/3/ca8620en/ca8620en.pdf (last access: 14 March 2023), 2020.

Ferreira, T. O., Vidal-Torrado, P., Otero, X. L., and Macías, F.: Are mangrove forest substrates sediments or soils?, A case study in southeastern Brazil, Catena, 70, 79–91, https://doi.org/10.1016/j.catena.2006.07.006, 2007.

Ferreira, T. O., Queiroz, H. M., Nóbrega, G. N., de Souza Júnior, V. S., Barcellos, D., Ferreira, A. D., and Otero, X. L.: Lithoclimatic characteristics and its control over mangrove soil geochemistry: A macro-scale approach, Sci. Total Environ., 811, 152152, https://doi.org/10.1016/j.scitotenv.2021.152152, 2022.

Ferronato, C., Falsone, G., Natale, M., Zannoni, D., Buscaroli, A., Vianello, G., and Vittori Antisari, L.: Chemical and pedological features of subaqueous and hydromorphic soils along a hydrosequence within a coastal system (San Vitale Park, Northern Italy), Geoderma, 265, 141–151, https://doi.org/10.1016/j.geoderma.2015.11.018, 2016.

Flemming, B. W.: A revised textural classification of gravel-free muddy sediments on the basis of ternary diagrams, Cont. Shelf Res., 20, 1125–1137, https://doi.org/10.1016/S0278-4343(00)00015-7, 2000.

Fourqurean, J. W., Duarte, C. M., Kennedy, H., Marbà, N., Holmer, M., Mateo, M. A., Apostolaki, E. T., Kendrick, G. A., Krause-Jensen, D., McGlathery, K. J., and Serrano, O.: Seagrass ecosystems as a globally significant carbon stock, Nat. Geosci., 5, 505–509, https://doi.org/10.1038/ngeo1477, 2012.

Furlan, A., Bonotto, D. M., and Gumiere, S. J.: Development of environmental and natural vulnerability maps for Brazilian coastal at São Sebastião in São Paulo State, Environ. Earth Sci., 64, 659–669, https://doi.org/10.1007/s12665-010-0886-7, 2011.

Furquim, S. A. C., Graham, R. C., Barbiero, L., de Queiroz Neto, J. P., and Vallès, V.: Mineralogy and genesis of smectites in an alkaline-saline environment of Pantanal wetland, Brazil, Clays Clay Miner., 56, 579–595, https://doi.org/10.1346/CCMN.2008.0560511, 2008.

Gee, G. W. and Bauder, J. W.: Particle-size analysis, in: Methods of soil analysis: Part 1 – Physical and mineralogical methods, Soil Science Society of America, Am. Soc. Agron., 383–411, 1986.

Giblin, A. E.: Pyrite formation in marshes during early diagenesis, Geomicrobiol. J., 6, 77–97, https://doi.org/10.1080/01490458809377827, 1988.

Green, E. P. and Short, F. T.: World Atlas of Seagrasses, UNEP-WCMC, Cambridge, 336 pp., 2003.

Holmer, M., Andersen, F. Ø., Nielsen, S. L., and Boschker, H. T. S.: The importance of mineralization based on sulfate reduction for nutrient regeneration in tropical seagrass sediments, Aquat. Bot., 71, 1–17, https://doi.org/10.1016/S0304-3770(01)00170-X, 2001.

Howard, J., Hoyt, S., Isensee, K., Telszewski, M., Pidgeon, E., and Telszewski, M.: Coastal blue carbon: methods for assessing carbon stocks and emissions factors in mangroves, tidal salt marshes, and seagrasses, Conservation International, Intergovernmental Oceanographic Commission of UNESCO, International Union for Conservation of Nature, Arlington, VA, USA, Arlington, VA, USA, 184 pp., 2014.

Inoue, T., Nohara, S., Takagi, H., and Anzai, Y.: Contrast of nitrogen contents around roots of mangrove plants, Plant Soil, 339, 471–483, https://doi.org/10.1007/s11104-010-0604-y, 2011.

IUSS Working Group WRB: World Reference Base for Soil Resources 2014, update 2015 International soil classification system for naming soils and creating legends for soil maps, FAO, Rome, 1–191 pp., 2015.

Jahn, R., Blume, H. P., Asio, V. B., Spaargaren, O., and Schad, P.: Guidelines for soil description, FAO, ISBN 92-5-105521-1, 2006.

Jimenez, L. C. Z., Queiroz, H. M., Nóbrega, G. N., Romero, D. J., Deng, Y., Otero, X. L., and Ferreira, T. O.: Recovery of soil pro-

cesses in replanted mangroves: implications for soil functions, Forests, 13, 422, https://doi.org/10.3390/f13030422, 2022.

Kennedy, H., Beggins, J., Duarte, C. M., Fourqurean, J. W., Holmer, M., Marbà, N., and Middelburg, J. J.: Seagrass sediments as a global carbon sink: Isotopic constraints, Global Biogeochem. Cy., 24, GB4026, https://doi.org/10.1029/2010GB003848, 2010.

Kida, M., Tomotsune, M., Iimura, Y., Kinjo, K., Ohtsuka, T., and Fujitake, N.: High salinity leads to accumulation of soil organic carbon in mangrove soil, Chemosphere, 177, 51–55, https://doi.org/10.1016/j.chemosphere.2017.02.074, 2017.

Konsten, C. J. M., Brinkman, R., and Andriesse, W.: A field laboratory method to determine total potential and actual acidity in acid sulphate soils, in: Selected papers of the Dakar symposium on acid sulphate soils: Dakar, Senegal, January 1986, 106–134, 1988.

Lacerda, L. D., de Menezes, M. O. T., and Molisani, M. M.: Changes in mangrove extension at the Pacoti River estuary, CE, NE Brazil due to regional environmental changes between 1958 and 2004, Biota Neotrop., https://doi.org/10.1590/s1676-06032007000300007, 2007.

Larcombe, P., Costen, A., and Woolfe, K. J.: The hydrodynamic and sedimentary setting of nearshore coral reefs, central Great Barrier Reef shelf, Australia: Paluma Shoals, a case study, Sedimentology, 48, 811–835, https://doi.org/10.1046/j.1365-3091.2001.00396.x, 2001.

Lehmann, J. and Kleber, M.: The contentious nature of soil organic matter, Nature, 528, 60–68, https://doi.org/10.1038/nature16069, 2015.

Lemos, R. C., Azolim, M. Â. D., Abrão, P. U. R., and Santos, M. C. L.: Levantamento de reconhecimento dos solos do Estado do Rio Grande do Sul, Ministério da Agricultura, Recife, 431 pp., 1973.

Lopes, R. P., Dillenburg, S. R., and Schultz, C. L.: Cordão formation: Loess deposits in the southern coastal plain of the state of Rio Grande do Sul, Brazil, An. Acad. Bras. Cienc., 88, 2143–2166, https://doi.org/10.1590/0001-3765201620150738, 2016.

Lord III, C. J.: A selective and precise method for pyrite determination in sedimentary materials, J. Sediment. Res., 52, 664–666, https://doi.org/10.1306/212F7FF4-2B24-11D7-8648000102C1865D, 1982.

Lowry, G. V., Espinasse, B. P., Badireddy, A. R., Richardson, C. J., Reinsch, B. C., Bryant, L. D., Bone, A. J., Deonarine, A., Chae, S., Therezien, M., Colman, B. P., Hsu-Kim, H., Bernhardt, E. S., Matson, C. W., and Wiesner, M. R.: Long-Term Transformation and Fate of Manufactured Ag Nanoparticles in a Simulated Large Scale Freshwater Emergent Wetland, Environ. Sci. Technol., 46, 7027–7036, https://doi.org/10.1021/es204608d, 2012.

Macías, F. and Camps-Arbestain, M.: A biogeochemical view of the world reference base soil classification system: Homage to Ward Chesworth, 1st ed., Elsevier Inc., 295–342, https://doi.org/10.1016/bs.agron.2019.11.002, 2020.

Marbà, N., Arias-Ortiz, A., Masqué, P., Kendrick, G. A., Mazarrasa, I., Bastyan, G. R., Garcia-Orellana, J., and Duarte, C. M.: Impact of seagrass loss and subsequent revegetation on carbon sequestration and stocks, J. Ecol., 103, 296–302, https://doi.org/10.1111/1365-2745.12370, 2015.

Mazarrasa, I., Marbà, N., Lovelock, C. E., Serrano, O., Lavery, P. S., Fourqurean, J. W., Kennedy, H., Mateo, M. A., Krause-Jensen, D., Steven, A. D. L., and Duarte, C. M.: Seagrass meadows as a globally significant carbonate reservoir, Biogeosciences, 12, 4993–5003, https://doi.org/10.5194/bg-12-4993-2015, 2015.

Melo, V. F., Novais, R. F., Schaefer, C. E. G. R., Fontes, M. P. F., and Singh, B.: Mineralogia das frações areia, silte e argila de sedimentos do grupo barreiras no município de Aracruz, estado do Espírito Santo, Rev. Bras. Ciência do Solo, 26, 29–41, https://doi.org/10.1590/s0100-06832002000100004, 2002.

Minuzzi, R. B., Sediyama, G. C., Barbosa, E. da M., and de Melo Júnior, J. C. F. : Climatologia do comportamento do período chuvoso da região sudeste do Brasil, Rev. Bras. Meteorol., 22, 338–344, https://doi.org/10.1590/S0102-77862007000300007, 2007.

Nobrega, G. N.: Subaqueous soils of the Brazilian seagrass meadows: biogeochemistry, genesis, and classification, Universidade de São Paulo, Piracicaba, 123 pp., https://doi.org/10.11606/T.11.2018.tde-26102017-143348, 2018.

Nóbrega, G. N., Ferreira, T. O., Romero, R. E., Marques, A. G. B., and Otero, X. L.: Iron and sulfur geochemistry in semiarid mangrove soils (Ceará, Brazil) in relation to seasonal changes and shrimp farming effluents, Environ. Monit. Assess., 185, 7393–7407, https://doi.org/10.1007/s10661-013-3108-4, 2013.

Nóbrega, G. N., Otero, X. L., Macías, F., and Ferreira, T. O.: Phosphorus geochemistry in a Brazilian semiarid mangrove soil affected by shrimp farm effluents, Environ. Monit. Assess., 186, 5749–5762, https://doi.org/10.1007/s10661-014-3817-3, 2014.

Nóbrega, G. N., Ferreira, T. O., Siqueira Neto, M., Queiroz, H. M., Artur, A. G., Mendonça, E. D. S., Silva, E. D. O., and Otero, X. L.: Edaphic factors controlling summer (rainy season) greenhouse gas emissions (CO_2 and CH_4) from semiarid mangrove soils (NE-Brazil), Sci. Total Environ., 542, 685–693, https://doi.org/10.1016/j.scitotenv.2015.10.108, 2016.

Nóbrega, G. N., Romero, D. J., Otero, X. L., and Ferreira, T. O.: Pedological Studies of Subaqueous Soils as a Contribution to the Protection of Seagrass Meadows in Brazil, Rev. Bras. Ciência do Solo, 42, 1–12, https://doi.org/10.1590/18069657rbcs20170117, 2018.

Nóbrega, G. N., Ferreira, T. O., Siqueira Neto, M., de Mendonça, E. S., Romero, R. E., and Otero, X. L.: The importance of blue carbon soil stocks in tropical semiarid mangroves: a case study in Northeastern Brazil, Environ. Earth Sci., 78, 369, https://doi.org/10.1007/s12665-019-8368-z, 2019.

Nollet, L. M. L. and De Gelder, L. S. P.: Handbook of water analysis, CRC press, 784 pp., 2000.

Ooi, J. L. S., Kendrick, G. A., Van Niel, K. P., and Affendi, Y. A.: Knowledge gaps in tropical Southeast Asian seagrass systems, Estuar. Coast. Shelf Sci., 92, 118–131, https://doi.org/10.1016/j.ecss.2010.12.021, 2011.

Orth, R. J., Carruthers, T. I. M. J. B., Dennison, W. C., Carlos, M., Fourqurean, J. W., Jr, K. L. H., Hughes, A. R., Kendrick, A., Kenworthy, W. J., Olyarnik, S., Short, F. T., Waycott, M., Williams, S. L. K. L. H., Hughes, A. R., Kendrick, G. A., and Kenworthy, W. J.: A Global Crisis for Seagrass Ecosystems, Bioscience, 56, 987–996, https://doi.org/10.1641/0006-3568(2006)56[987:AGCFSE]2.0.CO;2, 2006.

Osher, L. J. and Flannagan, C. T.: Soil/Landscape Relationships in a Mesotidal Maine Estuary, Soil Sci. Soc. Am. J., 71, 1323–1334, https://doi.org/10.2136/sssaj2006.0224, 2007.

Otero, X. L., Ferreira, T. O., Vidal-Torrado, P., Macias, F., and Chesworth, W.: Thionic Soils, edited by: Chesworth, W., Springer, Berlin, Encycl. Soil Sci., 777–780, 2008.

Otero, X. L., Ferreira, T. O., Huerta-Díaz, M. A., Partiti, C. S. M., Souza, V., Vidal-Torrado, P., and Macías, F.: Geochemistry of iron and manganese in soils and sediments of a mangrove system, Island of Pai Matos (Cananeia – SP, Brazil), Geoderma, 148, 318–335, https://doi.org/10.1016/j.geoderma.2008.10.016, 2009.

Payne, M. K. and Stolt, M. H.: Understanding sulfide distribution in subaqueous soil systems in southern New England, USA, Geoderma, 308, 207–214, https://doi.org/10.1016/j.geoderma.2017.08.015, 2017.

Peel, M. C., Finlayson, B. L., and McMahon, T. A.: Updated world map of the Köppen-Geiger climate classification, Hydrol. Earth Syst. Sci., 11, 1633–1644, https://doi.org/10.5194/hess-11-1633-2007, 2007.

Prada-Gamero, R. M., Vidal-Torrado, P., and Ferreira, T. O.: Mineralogia e físico-química dos solos de mangue do rio Iriri no canal de Bertioga (Santos, SP), Rev. Bras. Ciência do Solo, 28, 233–243, https://doi.org/10.1590/s0100-06832004000200002, 2004.

Pugliese Andrade, G. R., de Azevedo, A. C., Cuadros, J., Souza, V. S., Correia Furquim, S. A., Kiyohara, P. K., and Vidal-Torrado, P.: Transformation of Kaolinite into Smectite and Iron-Illite in Brazilian Mangrove Soils, Soil Sci. Soc. Am. J., 78, 655–672, https://doi.org/10.2136/sssaj2013.09.0381, 2014.

Queiroz, H. M., Ferreira, T. O., Fandiño, V. A., Bragantini, I. O. B. F., Barcellos, D., Nóbrega, G. N., Ferreira, A. D., Gomes, L. E. O., and Bernardino, A. F.: Changes in soil iron biogeochemistry in response to mangrove dieback, Biogeochem., 158, 357–372, https://doi.org/10.1007/s10533-022-00903-1, 2022.

Reimann, C., Filzmoser, P., Garrett, R. G., and Dutter, R.: Statistical Data Analysis Explained, John Wiley & Sons, Ltd, Chichester, UK, https://doi.org/10.1002/9780470987605, 2008.

Reverte, F. C. and da Garcia, M.: O patrimônio geológico de São Sebastião – SP: inventário e uso potencial de geossítios com valor científico, 35, 496–511, 2016.

Schaeffer-Novelli, Y., de Souza Lima Mesquita, H., Cintrón-Molero, G., and Cintron-Molero, G.: The Cananéia Lagoon Estuarine System, São Paulo, Brazil, 13, 193, https://doi.org/10.2307/1351589, 1990.

Schaetzl, R. J. and Thompson, M. L.: Soils: Genesis and Geomorphology, 2nd ed., Cambridge University Press, New York, NY, 795 pp., 2015.

Schmidt, M. W. I., Torn, M. S., Abiven, S., Dittmar, T., Guggenberger, G., Janssens, I. A., Kleber, M., Kögel-Knabner, I., Lehmann, J., Manning, D. A. C., Nannipieri, P., Rasse, D. P., Weiner, S., and Trumbore, S. E.: Persistence of soil organic matter as an ecosystem property, Nature, 478, 49–56, https://doi.org/10.1038/nature10386, 2011.

Schoeneberger, P. J., Wysocki, D. A., Benham, E. C., and Broderson, W. D.: Field Book for Describing and Sampling Soils, Natl. Soil Surv. Cent., 33, 1–228, 2002.

Seeliger, U.: The Patos Lagoon Estuary, Brazil, in: Coastal Marine Ecosystems of Latin America, Springer, 167–183, https://doi.org/10.1007/978-3-662-04482-7_ 13, 2001.

Serrano, O., Ricart, A. M., Lavery, P. S., Mateo, M. A., Arias-Ortiz, A., Masque, P., Rozaimi, M., Steven, A., and Duarte, C. M.: Key biogeochemical factors affecting soil carbon storage in Posidonia meadows, Biogeosciences, 13, 4581–4594, https://doi.org/10.5194/bg-13-4581-2016, 2016a.

Serrano, O., Lavery, P. S., Duarte, C. M., Kendrick, G. A., Calafat, A., York, P. H., Steven, A., and Macreadie, P. I.: Can mud (silt and clay) concentration be used to predict soil organic carbon content within seagrass ecosystems?, Biogeosciences, 13, 4915–4926, https://doi.org/10.5194/bg-13-4915-2016, 2016b.

Short, F., Carruthers, T., Dennison, W., and Waycott, M.: Global seagrass distribution and diversity: A bioregional model, J. Exp. Mar. Bio. Ecol., 350, 3–20, https://doi.org/10.1016/j.jembe.2007.06.012, 2007.

Short, F. T., Polidoro, B., Livingstone, S. R., Carpenter, K. E., Bandeira, S., Bujang, J. S., Calumpong, H. P., Carruthers, T. J. B., Coles, R. G., Dennison, W. C., Erftemeijer, P. L. A., Fortes, M. D., Freeman, A. S., Jagtap, T. G., Kamal, A. H. M., Kendrick, G. A., Judson Kenworthy, W., La Nafie, Y. A., Nasution, I. M., Orth, R. J., Prathep, A., Sanciangco, J. C., Tussenbroek, B. van, Vergara, S. G., Waycott, M., and Zieman, J. C.: Extinction risk assessment of the world's seagrass species, Biol. Conserv., 144, 1961–1971, https://doi.org/10.1016/j.biocon.2011.04.010, 2011.

Søndergaard, M.: Redox Potential, in: Encyclopedia of Inland Waters, Elsevier, 852–859, https://doi.org/10.1016/B978-012370626-3.00115-0, 2009.

Souza-Júnior, V. S., Vidal-Torrado, P., Garcia-Gonzaléz, M. T., Otero, X. L., and Macías, F.: Soil Mineralogy of Mangrove Forests from the State of São Paulo, Southeastern Brazil, Soil Sci. Soc. Am. J., 72, 848–857, https://doi.org/10.2136/sssaj2007.0197, 2008.

Souza-Júnior, V. S. de, Vidal-Torrado, P., Tessler, M. G., Pessenda, L. C. R., Ferreira, T. O., Otero, X. L., and Macías, F.: Evolução quaternária, distribuição de partículas nos solos e ambientes de sedimentação em manguezais do estado de São Paulo, Rev. Bras. Ciência do Solo, 31, 753–769, https://doi.org/10.1590/S0100-06832007000400016, 2007.

Souza-Júnior, V. S. de, Vidal-Torrado, P., Garcia-González, M. T., Macías, F., and Otero, X. L.: Smectite in mangrove soils of the State of São Paulo, Brazil, Sci. Agric., 67, 47–52, https://doi.org/10.1590/s0103-90162010000100007, 2010.

Środoń, J.: Nature of mixed-layer clays and mechanisms of their formation and alteration, Annu. Rev. Earth Planet. Sci., 27, 19–53, https://doi.org/10.1146/annurev.earth.27.1.19, 1999.

Still, B. M. and Stolt, M. H.: Subaqueous Soils and Coastal Acidification: A Hydropedology Perspective with Implications for Calcifying Organisms, https://doi.org/10.2136/sssaj2014.09.0366, 2015.

Sumner, M. E. and Miller, W. P.: Cation Exchange Capacity and Exchange Coefficients, in: Methods of soil analysis, Part 3 – chemical methods, 1201–1229, https://doi.org/10.2136/sssabookser5.3.c40, 2018.

Thorhaug, A., Poulos, H. M., López-Portillo, J., Ku, T. C. W., and Berlyn, G. P.: Seagrass blue carbon dynamics in the Gulf of Mexico: Stocks, losses from anthropogenic disturbance, and gains through seagrass restoration, Sci. Total Environ., 605, 626–636, https://doi.org/10.1016/j.scitotenv.2017.06.189, 2017.

Toldo Jr., E. E., Dillenburg, S. R., Corrêa, I. C. S., and Almeida, L. E. S. B.: Holocene Sedimentation in Lagoa dos Patos Lagoon, Rio Grande do Sul, Brazil, J. Coast. Res., 16, 816–822, 2000.

Van Reeuwijk, L. P.: Procedures for soil analysis, 6th Editio., ISRIC – World Soil Information, Wageningen, Netherlands, ISBN 90-6672-044-1, 2002.

Velde, B. and Church, T.: Rapid clay transformations in Delaware salt marshes, 14, 559–568, 1999.

Veneman, P. L. M., Spokas, L. A., and Lindbo, D. L.: Soil Moisture and Redoximorphic Features: A Historical Perspective, 1–23, https://doi.org/10.2136/sssaspecpub54.c1, 2015.

Vilas Bôas, G. S., Sampaio, F. J., and Pereira, A. M. S.: The Barreiras Group in the Northeastern coast of the State of Bahia, Brazil: depositional mechanisms and processes, An. Acad. Bras. Cienc., 73, 417–427, https://doi.org/10.1590/S0001-37652001000300010, 2001.

Vittori Antisari, L., De Nobili, M., Ferronato, C., Natale, M., Pellegrini, E., and Vianello, G.: Hydromorphic to subaqueous soils transitions in the central Grado lagoon (Northern Adriatic Sea, Italy), Estuar. Coast. Shelf Sci., 173, 39–48, https://doi.org/10.1016/j.ecss.2016.02.004, 2016.

Walker, D. and McComb, A.: Seagrass degradation in Australian coastal waters, Mar. Pollut. Bull., 25, 191–195, https://doi.org/10.1016/0025-326X(92)90224-T, 1992.

Weiss, J. V., Emerson, D., and Megonigal, J. P.: Geochemical control of microbial Fe(III) reduction potential in wetlands: comparison of the rhizosphere to non-rhizosphere soil, FEMS Microbiol. Ecol., 48, 89–100, https://doi.org/10.1016/j.femsec.2003.12.014, 2004.

Wessel, B. M., Rabenhorst, M. C., and Needelman, B. A.: A subaqueous soil-landscape conceptual model to guide soil survey in Chesapeake Bay subestuaries, Soil Sci. Soc. Am. J., 85, 1727–1740, https://doi.org/10.1002/saj2.20305, 2021.

Zarnoch, C. B., Hoellein, T. J., Furman, B. T., and Peterson, B. J.: Eelgrass meadows, *Zostera marina* (L.), facilitate the ecosystem service of nitrogen removal during simulated nutrient pulses in Shinnecock Bay, New York, USA, Mar. Pollut. Bull., 124, 376–387, https://doi.org/10.1016/j.marpolbul.2017.07.061, 2017.